國 立 交 通 大 學
光 電 工 程 研 究 所

碩 士 論 文

氮化鎵二維光子晶體面射型雷射之
雷射行為研究

The Study of lasing behavior in GaN-based 2D Photonic Crystal Surface Emitting Lasers

研究生：劉 亭 均

指導教授：郭 浩 中 教授

盧 廷 昌 教授

中華民國九十八 年六月

氮化鎵二維光子晶體面射型雷射之雷射行為研究

The Study of Lasing Behavior in GaN-Based 2D Photonic Crystal Surface Emitting Lasers

研 究 生：劉亭均 　　　　 Student：Ting-Chun Liu

指導教授：郭浩中 　　　　 Advisors：Hao-Chung Kuo

　　　　 盧廷昌 　　　　　　　　　　 Tien-Chang Lu

國 立 交 通 大 學

光 電 工 程 研 究 所

碩 士 論 文

A Thesis

Submitted to Institute of Electro-Optical Engineering

College of Electrical Engineering and Computer Science

National Chiao Tung University

in partial Fulfillment of the Requirements

for the Degree of Master

in

Electro-Optical Engineering

June 2009

Hsinchu, Taiwan, Republic of China

中 華 民 國 九 十 八 年 六 月

氮化鎵二維光子晶體面射型雷射之雷射行為研究

研究生: 劉亭均

指導教授: 郭浩中 教授
盧廷昌 教授

國立交通大學 光電工程研究所

摘　要

本篇論文旨在探討不同的光子晶體週期造成不同特性的氮化鎵二維光子晶體面射型雷射。根據光子晶體週期性結構的布拉格理論，光子晶體的雷射出射必須滿足特定的布拉格繞射條件。因此我們利用平面波展開法模擬 TE 能帶圖設計光子晶體元件之晶格常數範圍從 190 到 230 奈米，並且製作光子晶體週期性結構於氮化鎵共振腔發光二極體。藉由脈衝雷射激發，此結構可以激發出光子晶體雷射。從實驗數據研究光子晶體雷射之正規化頻率正好相對於 TE 能帶圖三個能帶邊界($\Gamma 1$，$K2$，$M3$) ，表示雷射只發生在特定能帶的邊界上。將不同的能帶邊界雷射所得的變角度光致發光光譜圖與能帶圖相互比對，直接量測能帶與雷射點的交會，更加證實雷射發生在($\Gamma 1$，$K2$，$M3$) 此三個能帶邊界。由實驗數據可知，$\Gamma 1$，$K2$ 及 $M3$ 的出射角度相對於垂直出射角分別為 $0°$, $29°$及 $59.5°$；$\Gamma 1$，$K2$ 及 $M3$ 的雷射極化程度和發散角分別為 $(33\%, 35\%, 55\%)$ 及 $(1.2°, 2.5°, 2.2°)$ 。此外，我們觀測到 $\Gamma 1$ 模態的遠場為對稱圖形，正好與光子晶體的對稱型結構相符。由於氮化鎵光子晶體雷射具有許多優越的光學特性，我們相信此結構可以應用在可見光及藍紫光雷射等高功率、大範圍及多用途之光電元件中。

The Study of Lasing Behavior in GaN-based 2D Photonic Crystal Surface Emitting Lasers

Student : Ting-Chun Liu   Advisor: Huo-Chung Kuo

Tien-Chang Lu

Institute of electro-optical Engineering

National Chiao-Tung University

Abstract

In this thesis, we investigated the different lasing behavior of GaN-based 2D photonic crystal surface emitting lasers (PCSELs) according to different photonic crystal (PhCs) lattice constant. Based on the Bragg theory for PhCs period structure, the lasing behavior could only happen when the Bragg condition is satisfied. Therefore, we simulated the band diagram of TE mode by plane wave expansion method, designed the PhCs lattice constant ranging from 190 to 230 nm, and fabricated the PhCs period structure on our novel GaN-based resonance cavity light emitting diode. By the excitation of pulse laser, the PhCs lasing action is achieved under the optical pumping system. Normalized frequency of investigated PCSELs lasing wavelength can be correspond to three band-edge frequencies (Γ1, K2, M3), which indicates the lasing action can only occur at specific band-edges. We also measured the angle-resolved μ-PL diagrams of different lasing modes. The results further confirmed the lasing modes existed at different band-edge (Γ1, K2, M3) and emitted different lasing angles by mapping the diffraction patterns of band structures and the Bragg theory. From our experiment results, the three band-edge frequencies including Γ1, K2, and M3 has different emission angles corresponding to the normal direction (0˚, 29˚, 59.5˚), respectively. Moreover, the far field pattern of Γ1 mode we observed is symmetric due

to the PhCs' symmetric pattern structure. Besides, the degree of polarizations and divergence angles of $\Gamma 1$, K2, and M3 modes laser are about (33%, 35%, 55%) and (1.2˚, 2.5˚, 2.2˚), respectively. Overall, according to the superiority features of GaN-based PCSELs, the structure can be applied in the visible and UV laser and become the highly potential optoelectronic device in high power emitter applications.

誌謝

又到了鳳凰花開的季節，碩士班兩年的時光匆匆飛逝。回想到剛踏進交大校門時的不安與期待，到進了 "S.C. Lab" 開始瞭解甚麼是半導體，現在即將帶著畢業證書走出實驗室、踏出交大。其中當然是喜怒哀樂百感交集，幸好有師長、學長姐、同學以及學弟妹們的扶持與鼓勵，才讓我能在這裡感謝他們！

首先要感謝盧廷昌老師與郭浩中老師，老師每每在我碰壁時給我方向、線索，讓我學著以邏輯性與嚴謹的方法解決問題並得到可靠的實驗結果。我的直屬學長士偉、宗鼎、子維，學長們教導我實驗上的種種，當我遇到挫折時也深感其受一起幫我想解決之道，尤其在深夜還不離不棄地陪我做實驗…真是太感人了！也很感謝明學、清華學長，不僅在學術方面幫助我並帶我 explore 新竹，讓很沒有方向感以及探險精神的我可以嚐遍美食~！感謝學姐昀恬，幫我找到人生的第一份工作！同學梅君、阿綱、柯柯、董ㄟ、QQ、啄木、生哥、治凱、尚樺，在這兩年的互相扶持特別是課程內容的交流…，哈。直屬學弟哭哭、祥祥、翁翁翁，你們總是提出一些好方法，一步步的改善實驗方法幫了我很大的忙！感謝實驗室的所有人，感謝你們在我碩士生活中注入了一道道的溫暖，讓我在身處異鄉時並不感覺孤單、寂寞。

最後要感謝我的家人以及男朋友，總是無條件的支持我、鼓勵我。在我最消沉的時候幫我打氣，使我有勇氣再戰一回。你們是我努力向上最大的動力，很愛你們也很感謝你們喔！

學生 亭均 于 2009/07

Contents

Chapter 4   Optical Characteristics of GaN-based 2D Photonic Crystal Surface Emitting Lasers

Figure Contents

Chapter 1

Introduction

1-1 Nitride-based materials

Over the past few decades, nitride-based materials has been attracting much attentions because of their large direct wide band-gap characteristics and their various application in optoelectronic devices such as the backlight of flat panel displays, optical storage, lighting in automobiles, illumination and so on[1-4]. According to the large band off-set characteristic of these kinds of III-V wide band-gap materials, we expect the material which can be utilized in hetero-structure and provided better carrier confinement to increase the efficiency of the whole structure. Besides, the III-V materials have large band-gap characteristic ranging from sub-eV to several eV. It presents the material can emit the full visible light. Therefore, it is the promising potential to construct full-color display and solid-state lighting by light emitting diodes (LEDs) and laser diodes (LDs) fabricated by III-V materials. Furthermore, the characteristic of wide band-gap materials has larger dielectric strength (higher voltage per unit thickness) and strong excitonic energy which can be applied in more compact and higher frequency devices. Moreover, there are other advantages of these kinds of semiconductor with large band-gap that are not mention in previous describe such as
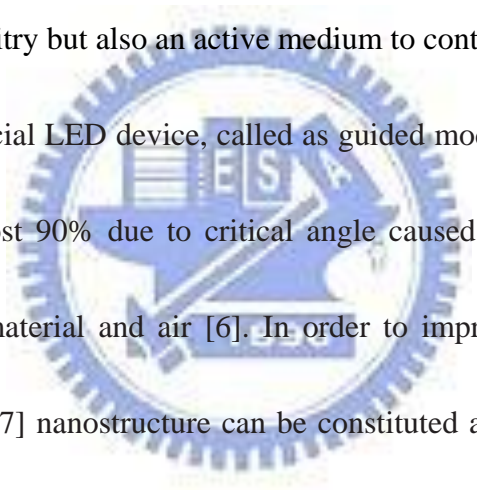
operation in higher temperature and the higher peak drift velocity of III-V materials

for electron. Especially in GaN, the material shows faster characteristic than that of Si

and GaAs (10^7 cm/s). Because of these advantages, the GaN-based devices play an

important role of the high efficiency electro-optic applications and products. However,

the problems in GaN, AlN, and its alloy materials are including large defect densities,

piezoelectric field effect and spontaneous polarization. It reveals the most important

thing is growing defect-free materials to fabricate high quality and high power devices.

Nowadays, there are many fundamental process armed at the breakthrough on how to

control defects, threading dislocation, lattice mismatch in epitaxy. Finally, as we

expect, the GaN-based materials with its superior properties make it a excellent

candidate for the optoelectronic applications in next decades.
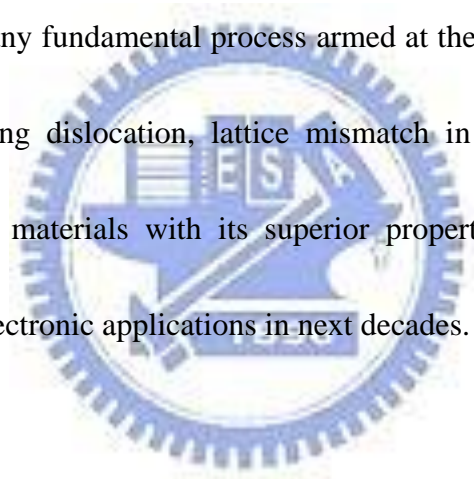
1-2 Photonic crystal in nitride-based materials

As we know, photonic crystal (PhC) is a dielectric structure arranged in periodic

geometry. Therefore, photonic crystal can exhibit one or more photonic band gaps

(PBGs), like a crystalline solid in electronic band structure, made some specific

frequencies in PBGs unable to propagate in the crystal, and have been drawing much

attention as new optical materials According to the PBGs phenomenon and/or the

dispersion relation between the photon energy and the wave vector, PhC

nanostructure for photons have many advantages in controlling the light emission arbitrarily, wave propagate along specific direction and can be utilized in realization of various new optoelectronic devices and/or circuits. For instance, PhC waveguide plays the role as a low loss channel for light propagation and resonator. Also maintain the whole cavity with high Q characteristic, which can be a promising device in conjunction with Si-based and III-V materials communication system. Semiconductor with these unique properties can not only be used as a versatile building block to construct photonic circuitry but also an active medium to control light emission [5].

Light in a commercial LED device, called as guided modes, would be trapped in the LED structure almost 90% due to critical angle caused by the refractive index different between the material and air [6]. In order to improve the light extraction from the devices, PhC [7] nanostructure can be constituted a promising candidate to increase the light extraction efficiency [8]. Besides, PhC is one of the most widely approach used in light emitting diode (LED) especially in nitride-based materials. Several technologies have been incorporated with PhC nanostructure to be the "light extractors", notably for GaN materials [9]. In 2005, Nakamura *et al.* reported a method to observe the band structure and the light extraction from PhC in GaN, and was an exactly evidence of a diffractive element caused by the three-dimensional (3-D) structure [10]. In this report, they also pointed out that there are two main ways to

improve light extraction from the devices by means of PhC nanostructure: one is using the PhC band gaps to prevent the emission light propagate in guided modes. The approach is challenging due to the method which needs to combine wavelength-sized microcavities with efficient electrical/optical injection and reduces the effect of nonradiative losses [11,12]; the other one uses the PhC nanostructure to couple guided modes to radiative modes [13,14]. Hence, most of the efficient extraction mechanism would be the second option because the use of 2-D PhC nanostructure would turn guided modes into radiative pseudo-guided Bloch modes, lying above the light line caused by air and material.

1-3 Photonic Crystal Lasers

Since photonic crystal is an artificial crystal, we can design different band structures only by varying the radius of holes (r) and lattice constant (a). Therefore, PhC could acts like either mirror or resonator only by varying the r/a ratio which is suitable for semiconductor lasers. In 1946, Edward Purcell first proposed that spontaneous emission from excited states of an atom can be significantly altered by placing it in a low loss cavity with dimensions on the order of the electromagnetic wavelength [15]. Recently, with the advent of semiconductor laser and the improvement of crystal growth and fabrication, there has been increasing more

interest in engineering of optical micro-cavity in semiconductor for light emission

control.

In general, there are two types of PhC lasers which has been investigated and

fabricated over the past few decades. The first one has a defect with optical gain

surrounded by a PhC mirror to form a resonant cavity. According to the photonic band

gap caused by the PhC nanostructure, light would be confined in the defect and lasing

actions would be arisen from the defect. This kind of PhC laser is called as photonic

crystals nano-cavity laser. The other one, called photonic crystal band edge laser, can

operate without any defined cavity and extrinsic PhC mirror. Therefore, the laser can

operate in the band edge region of the PhC band diagram. Finally, we can observe the

lasing phenomenon from the photonic crystal devices.

1-3.1 Photonic Crystal Nano-cavity Lasers

In 1994, P. R. Berman *et al.* first presented the mechanism that photonic crystal

could be a reflective mirror to form a cavity and achieve the laser operation [16].

Then, in 1999, O. Painter practically demonstrated an optically pumped

InGaAs-based 2-D PhC nano-cavity laser emitting at 1.55 micrometers [17]. The

optical cavity he demonstrated was consisted of a half-wavelength-thick waveguide

for vertical confinement and a 2-D PhC mirror for lateral localization. A defect was

introduced as a nano-cavity because the mode volume was 2.5 cubic half-wavelength

widths, approximately 0.03 micrometers, in the 2-D PC to trap photons inside. In 2004, H. G. Park *et al.* realized the electrically driven single-cell 2-D PhC laser with a dominated wavelength at 1519.7 nm [18]. They used a sub-micrometer-sized semiconductor post located at the center of the single-cell photonic crystal resonator to connect bottom electrode and achieved lasing action by current injection. The result is the first current injection report in the world.

However, the nitride-based photonic crystal nano-cavity laser never be observed in recently few decades. Fortunately, in 2005, nitride-based photonic crystal nano-cavity membrane emitted at 488nm with quality factor Q of about 800 was reported by Y. S. Choi *et al.* [19]. They used photo-enhanced chemical etching to form a GaN-based membrane with a total thickness of nearly 140 nm and patterned a photonic crystal nano-cavity on it. Some resonance modes from the nano-cavity with photonic crystal lattice constant of about 180 nm could be observed in the photoluminescence (PL) emission.

1-3.2 Photonic Crystal Band-edge Lasers

The second one is the photonic crystal band-edge lasers. According to the DFB theory, light at the photonic band-edge has zero group velocity and forms a standing wave due to 2-D DFB effect. Specific band-edges induce not only in-plane coupling via DFB, but also diffraction normal to the PhC plane, causing surface emission

phenomena. In 1999, Noda *et al.* reported the electrically driven 2-D PhC band-edge laser under pulsed operation [20]. The PhC nanostructure was a triangular-lattice structure composed of InP and air holes, which is integrated with an InGaAsP/InP multiple-quantum-well active layer by a wafer fusion technique. They demonstrated the single-mode, large-area and surface-emitting lasing action, and analyzed the lasing mechanism based on the satisfying of Bragg condition. Then, they further reported the room-temperature (RT) 2-D PhC band-edge laser under continuous wave (CW) operation in 2004 [21]. This opens a new road toward the large-area single-mode surface emitting laser. In 2008, Noda's group had demonstrated the GaN PCSELs room temperature operation by current injection; they also measured the angle-resolved diagram around Γ band-edge mode [22].
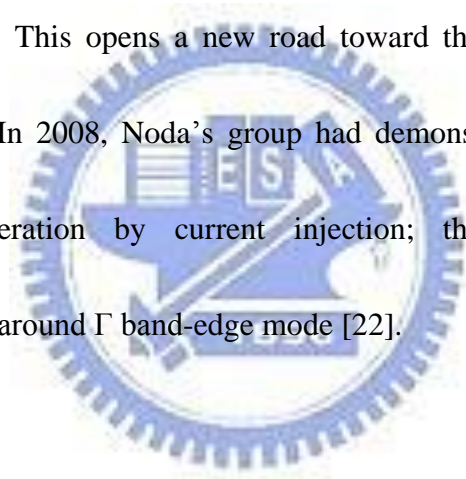
1-4 Objective of the thesis

During the past few decades, a considerable amount of literature about photonic crystal surface emitting lasers utilizing a 2-D distributed feedback (DFB) mechanism has been published and reported. Many relative works have been researched and focused on how to calculate photonic band-gap and the electric or magnetic field distribution in the photonic crystal nanostructure. Up to date, there are some previous researches and reports about using Bragg theory to explain the light extraction

enhancement from photonic crystal LED and lasing modes including Γ fundamental mode and high order modes arisen from photonic crystal surface emitting lasers (PCSELs). In this thesis, we have successfully fabricated the photonic crystal surface emitting lasers including three different types of band-edge modes such as Γ, M, and K modes in GaN-based 2-D PCSELs with AlN/GaN distributed Bragg reflectors (DBR). The AlN/GaN DBR structure plays the role as a low refractive index layer compared with GaN-based PCSELs which can confine the light field in the whole PCSEL structure. Therefore, we can obtain the fundamental Γ mode and high order modes of PC lasers. And then, we focused on the resonance cavity route, and the emission mechanisms, and laser operation behavior including lasing emission angle by angular-resolved μ-PL system, divergence angle, polarization, and far-field pattern of PCSELs by using Bragg theory. The relative characteristic of GaN-based PCSELs, especially in photonic crystal band-edge lasers, would be detail described the whole story in the following sections.

1-5 Outline of the thesis

This thesis is organized in the following arrangement. The first chapter introduces the history of GaN materials and the different types of photonic crystal surface emitting lasers in GaN-based materials. Chapter 2 introduces the Bragg theory

in 2D triangular lattice PhC causing different lasing properties of PhC lasers. Chapter 3 describes the wafer preparation and fabrication process of PCSELs. Chapter 4 presents the experimental analysis results and simulations of PCSELs. The last chapter shows the conclusion and future work.

References

[1] S. Nakamura, M. Senoh, N. Iwasa, and S. Nagahama, *Jpn. J. Appl.Phys.*, **34**, L797 (1995)

[2] S. Nakamura, T. Mukai, and M. Senoh, *Appl. Phys. Lett.*,**64**, 1687 (1994)

[3] S. Nakamura, M. Senoh, S.Nagahama, N.Iwasa, T. Yamada, T. Matsushita, Y. Sugimoto, and H.Kiyoku, *Appl. Phys. Lett.*, **70**, 868 (1997)

[4] S. Nakamura, *Science*, **281**, 956 (1998)

[5] C. M. Lai, H. M. Wu, P. C. Huang, S. L. Peng, *Appl. Phys. Lett.*, **90**, 141106, (2007)

[6] H. Benisty, H. De Neve, and C. Weisbuch, *IEEE J. Quantum Electron.* **34**, 1612 (1998); **34**, 1632 (1998).

[7] E. Yablonovitch, *Phys. Rev. Lett.* **58**, 2059 (1987).

[8] M. R. Krames, M. Ochiai-Holcomb, G. E. Holfer, C. Carter-Coman, E. I. Chen, I. H. Tan, P. Grillot, N. F. Gardner, H. C. Chui, J. W. Huang, S. A. Stockman, F. A. Kish, M. G. Craford, S. T. Tan, C. P. Kocot, M. Hueschen, J. Posselt, B. Loh, G. Sasser, and D. Collins, *Appl. Phys. Lett.* **75**, 2365 (1999).

[9] T. N. Oder, J. Shakya, J. Y. Lin, and H. X. Jiang, *Appl. Phys. Lett.* **83**, 1231 (2003).

[10] A. David, C. Meier, R. Sharma, F. S. Diana, S. P. DenBaars, E. Hu,

S. Nakamura, and C. Weisbuch, *Appl. Phys. Lett.* **87**, 101107 (2005).

[11] S. Fan, P. R. Villeneuve, J. D. Joannopoulos, and E. F. Schubert,

Phys. Rev. Lett. **78**, 3294 (1997).

[12] R. K. Lee, Y. Xu, and A. Yariv, *J. Opt. Soc. Am. B* **17**, 1438 (2000).

[13] M. Rattier, H. Benisty, R. P. Stanley, J.-F. Carlin, R. Houdré, U. Oesterle,

C. J. M. Smith, C. Weisbuch, and T. F. Krauss, *IEEE J. Sel. Top. Quantum*

Electron. **8**, 238 (2002).

[14] H. Rigneault, F. Lemarchand, and A. Sentenac, *J. Opt. Soc. Am. A* **17**, 1048

(2000).

[15] E.M. Purcell *Phys. Rev.* 69, 681 (1946)

[16] P. R. Berman, New York:Academic, (1994)

[17] O. Painter, R. K. Lee, A. Scherer, A. Yariv, J. D. O`Brien, P. D. Dapkus, I. Kim,

Science, **284**, 1819, (1999)

[18] H. G. Park, S. H. Kim, S. H. Kwon, Y. G. Ju, J. K. Yang, J. H. Baek, S. B. Kim, Y.

H. Lee, *Science*, **305**, 1444, (2005)

[19] Y. S. Choi, K. Hennessy, R. Sharma, E. Haberer, Y. Gao, S. P. DenBaars,

C. Meier, *Appl. Phys. Lett.*, **87**, 243101, (2005)

[20] M. Imada, S. Node, A. Chutinan. and T. Tokuda, *Appl. Phys. Lett.*, **75**,

316, (1999)

[21] D. Ohnishi, T. Okano, M. Imada, and S. Node, *Opt. Exp.,* **12**, 1562, (2004)

[22] Hideki Matsubara, Susumu Yoshimoto, Hirohisa Saito, Yue Jianglin, Yoshinori

Tanaka, Susumu Noda, *Science*, **319**, 25 JANUARY, (2008)

Chapter 2

Fundamental theory of Photonic Crystal

Surface Emitting Lasers

Introduction

Photonic crystal (PhC) surface emitting lasers utilizing a 2-D distributed feedback (DFB) mechanism has a considerable amount of publication during the past few years [1-4]. The PhC lasers have such excellent advantages to attract the people's attention including controlling the specific lasing modes such as longitudinal and transverse modes, lasing over the large area, and narrow divergence beam. Besides, the calculation of the photonic band-gap and the distribution of electric or magnetic field became more and more important. In the past few years, there were many theoretical calculations and methods have been developed, such as 2-D plane wave expansion method (PWEM) [2, 5], finite difference time domain (FDTD) [6, 7], transfer matrix method, and multiple scattering method, etc. However, there is no any detail lasing characteristic of PhC band-edge modes including the diagram of angular-solved μ-PL system, and the feature of high order lasing modes. In this thesis, we focused on the lasing behavior of PhC band-edge modes lasers in GaN-based 2-D PCSELs with AlN/GaN distributed Bragg reflectors. Each of PhC band-edge modes

exhibits a different type of wave coupling mechanism according to the Bragg diffraction mechanism. In this chapter, we introduced the fundamental and higher order Bragg diffraction in Chapter 2.1 and 2.2, respectively. According to Bragg diffraction mechanism, we expected the fundamental and high order PhC lasing modes which have specific lasing emission angles normally from the sample surface.

2-1 First order Bragg diffraction in 2-D triangular lattice PhC [8, 9]

Fig 2-1(a) shows a band diagram of PhC with triangular lattice. The points (A), (B), (C), (D), (E), and (F) are presented the different lasing modes including Γ_1, K_1, M_1, Γ_2, K_2, and M_2 respectively. Each of the different PhC band-edge lasing modes represents the PhC nanostructure can control the light propagated in different lasing wavelength and band-edge region. Fig 2-1(b) shows a schematic diagram in a reciprocal space. The reciprocal space of the PhC nanostructure is a space transferred by hexagonal photonic crystal nanostructure in real space. The K_1 and K_2 are the Bragg vectors with the same magnitude, $|K|=2\pi/a$, where a is the lattice constant of the photonic crystal. Considered the TE modes in the 2-D photonic crystal nanostructure, the diffracted light wave from the PhC structure must satisfy the Bragg's law and energy conservation:

$$k_d = k_i + q_1 K_1 + q_2 K_2, \qquad q_{1,2} = 0, \pm 1, \pm 2, ... \qquad (2.1)$$

$$\omega_d = \omega_i \qquad\qquad (2.2)$$

where k_d is a xy-plane wave vector of diffracted light wave; k_i is a xy-plane wave

vector of incident light wave; $q_{1,2}$ is order of coupling; ω_d is the frequency of

diffracted light wave, and ω_i is the frequency of incident light wave. Eq. (2.1)

represents the phase-matching condition (or momentum conservation), and Eq. (2.2)

represents the constant-frequency condition (or energy conservation). When both of

equations are satisfied, the lasing behavior would be observed.
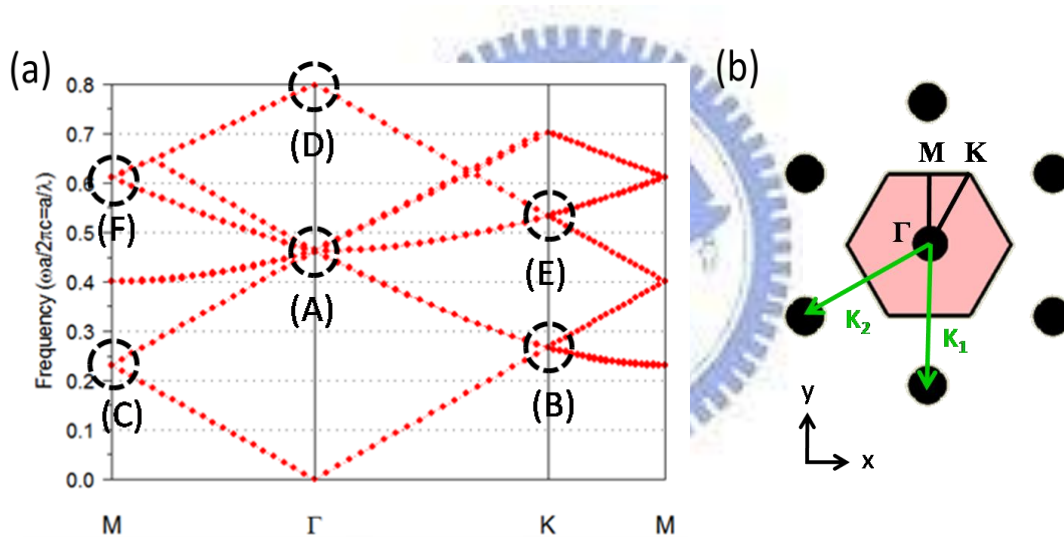
Figure 2-1(a) The band diagram of photonic crystal with triangular lattice; (b) The schematic diagram of photonic crystal with triangular lattice in reciprocal space.

Of course, it is expected the lasing behavior would occurs at specific points on

the Brillouin-zone boundary including Γ, M, and K and these PhC band-edge lasing

modes would split and cross. At these PhC lasing band-edge modes, waves

propagating in different directions would be coupled and increased the mode density

-15-

(or density of state, DOS). It is particularly interesting that each of these band-edge

modes exhibits a different type of wave coupling routes For example, as shown in Fig

2-1(c), the coupling at point(C) only involves two waves, propagating in the forward

and backward directions. This coupling is similar to that of a conventional DFB laser.

Both of them show the similar coupling mechanism but different lasing behavior

according to the different structure. However, there can be six equivalent Γ-M

directions in the structure; that is, the cavity can exist independently in each of the

three different directions to form three independent lasers. Point (B) has a unique

coupling characteristic which is different resonance mechanism compared with the

conventional DFB lasers. The coupling waves propagating in three different

directions are shown in Fig 2-2(b). This figure means that the cavity is a triangular

shape. On the other hand, the point (B) can also be six Γ-K directions in the structure.

Therefore, two different lasing cavities in different Γ-K directions coexist

independently. At point (A) in Fig 2-2(a), the coupling waves in in-plane are

including six directions 0°, 60°, 120°, -60°, -120°, and 180. The coupled light can

emit perpendicular from the sample surface according to satisfied first order Bragg

diffraction, as shown in Fig 2-3. Therefore, the PhC devices can function as a surface

emitting lasers.
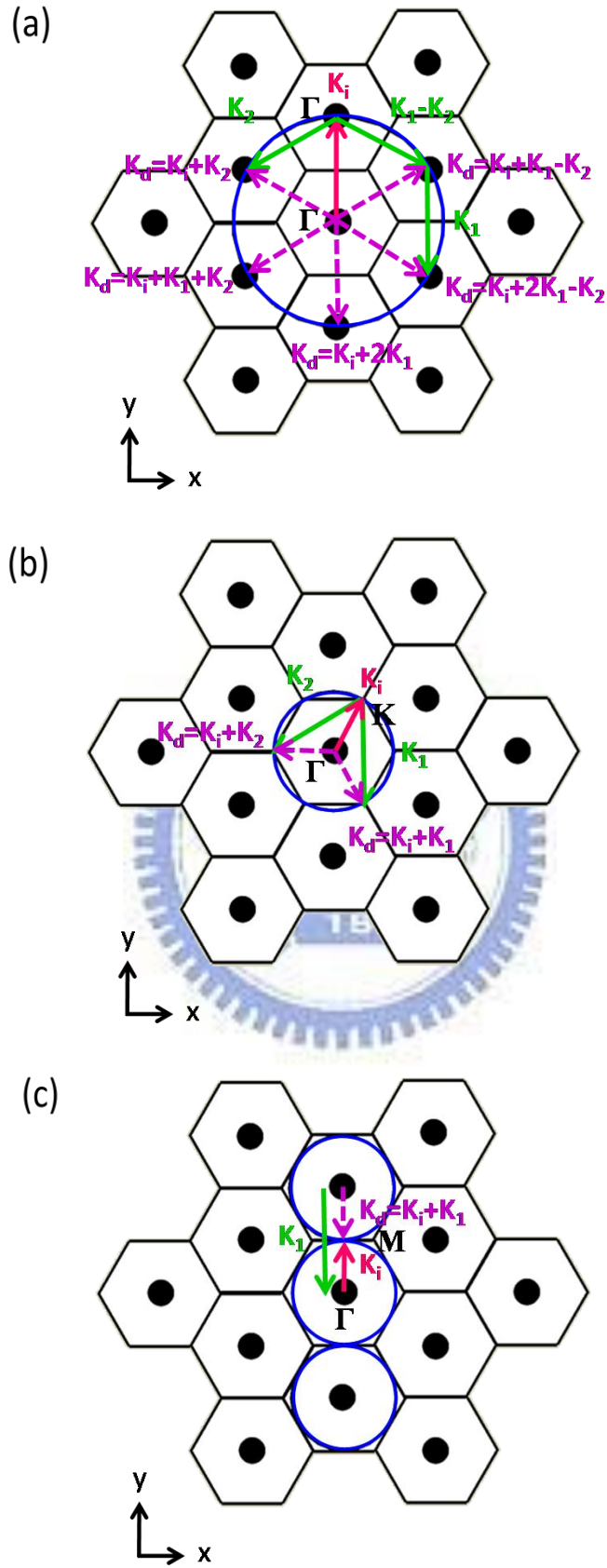
Figure 2-2 Wave vector diagram at points (A), (B), (C) in Figure 2-1(a); k_i and k_d indicate the incident and diffracted light wave.

-17-
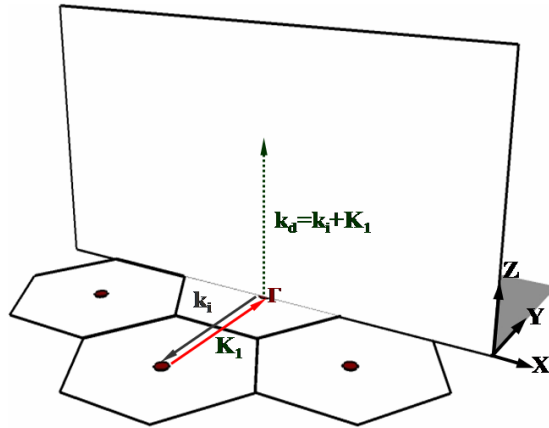
Figure 2-3 The wave vector diagram at point (A) in vertical direction.

2-2 Higher order Bragg diffraction in 2-D PhC with triangular lattice

Fig 2-4(a) and Fig 2-4(b) show the in-plane and vertical diffraction at point (D). In this case, the light wave is diffracted in five Γ-K directions and in the vertical direction similar to point (A) and $(K_i+q_1K_1+q_2K_2)$ which can reach to the six Γ' points. Figure 2-4(c) shows the wave vector diagram of one Γ' point in K space where the light wave is diffracted to an oblique direction. The light wave would be also diffracted to a bottom oblique direction.
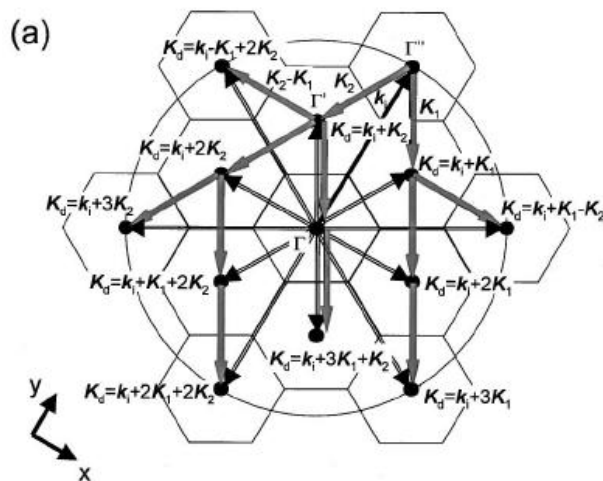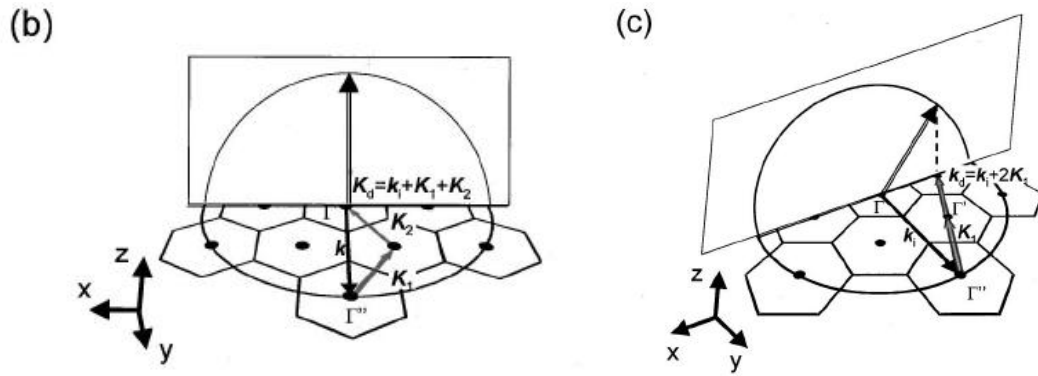
Figure 2-4 Wave vector diagram of (a) in-plane and (b) vertical direction at point (D); (c) wave vector diagram showing diffraction to an oblique direction at point (D).

Fig 2-5(a) and (b) show the in-plane and vertical diffraction at point (E). In this case, the light wave is diffracted in three Γ-K directions and $(K_i+q_1K_1+q_2K_2)$ which can reach to the three K' points. Fig 2-5(b) shows the wave-vector diagram of one K' point where the light wave is diffracted to an angle tilt 30° normally from the sample surface. Therefore, we expect the lasing behavior of K_2 mode that would emit at this specific angle.

(b)
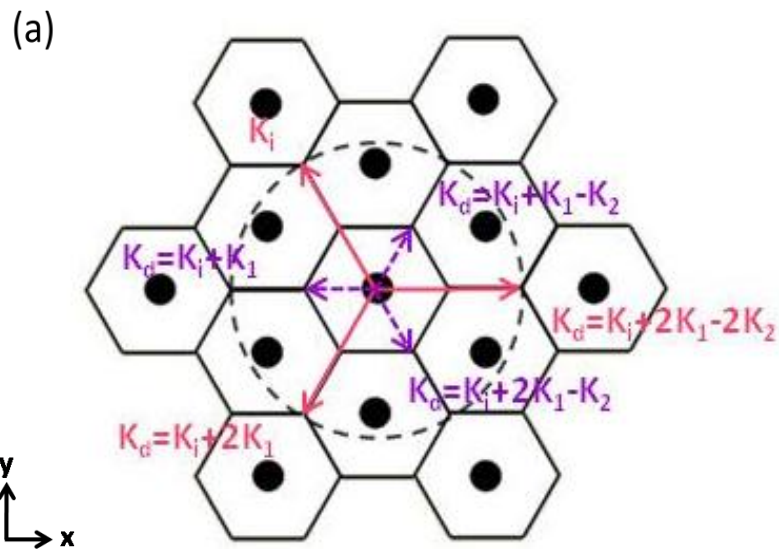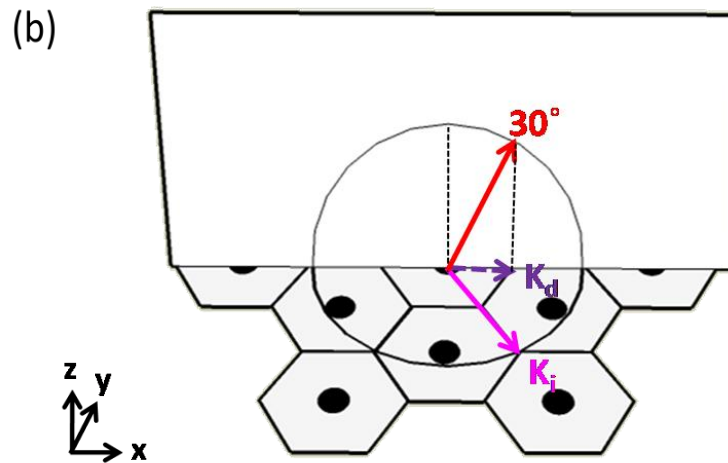
Figure 2-5 Wave vector diagram of (a) in-plane and (b) vertical direction at point (E) (or K2 mode); k_i and k_d indicate incident and diffracted light wave.

Fig 2-6(a) and (b) show the in-plane and vertical diffraction at point (F). In this case, the light wave is diffracted in two different Γ-M directions and $(K_i+q_1K_1+q_2K_2)$ which can reach to the three M' points. Fig 2-6(b) shows the wave-vector diagram of one M' point where the light wave is diffracted into three independent angles tilted of about $19.47°$, $35.26°$, and $61.87°$ normally from the sample surface, respectively. Since we collected PL spectrum on one detected plane, these diffraction angles would be happened on different detected planes. In our experiment, we could only detect one diffraction angle at one time limited by the detector when the PhC effect is occurred.
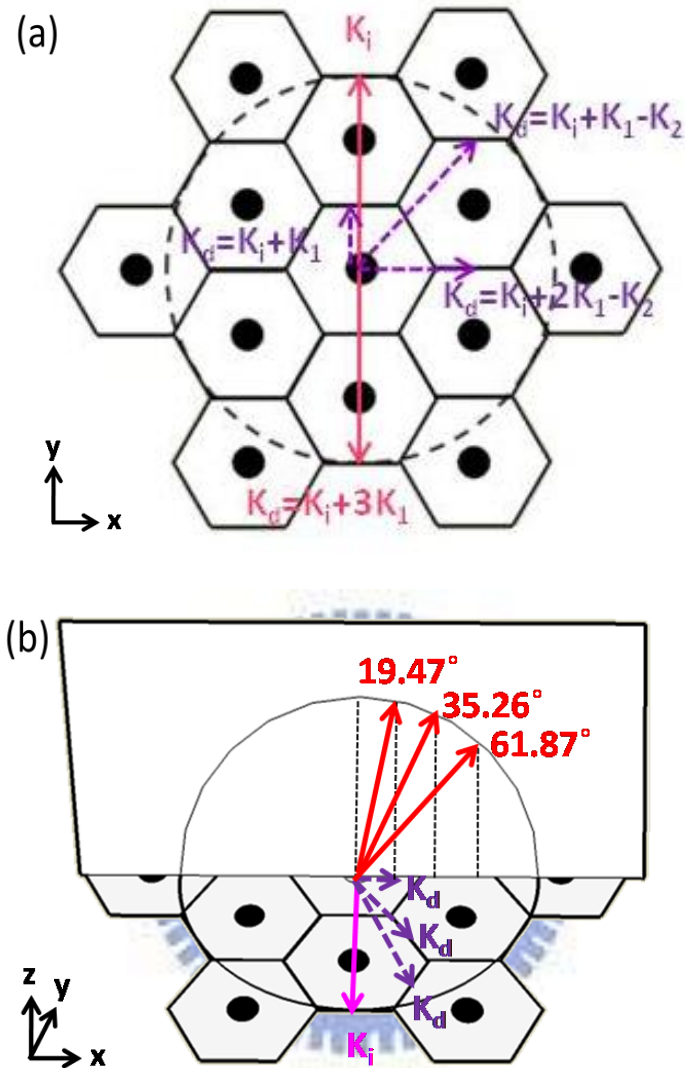
Figure 2-6 Wave vector diagram of (a) in-plane and (b) vertical direction at point (F) (or M3 mode); k_i and k_d indicate incident and diffracted light wave.

2-3 Diffraction pattern of 2-D PhC [10]

In the previous section, we show the Bragg diffraction mechanism causing different PhC lasing resonance routes including Γ mode and high order modes in K space. Furthermore, in this section, we will discuss about the "continuous" Bragg

diffraction extraction mechanism causing different diffraction lines in the diagram of angular-resolved μ-PL system. Each direction of emission (or extraction) is associated with a given in-plane wave vector, $k_{//}$, or effective index $n_{\text{eff}} = (k_{//})/k_0$, where k_0 is the wave vector of light in vacuum [11]. Therefore, the diagram by angular-resolved μ-PL system can be discussed and classified into four different parts by $n_{\textit{eff}}$ as shown in Figure 2-7(a). The parts of the spectrum with effective index $n_{\text{eff}} < 1$ are extracted directly. These propagate in all directions in air and represent only 10% of the whole radiated power. The parts with $1 < n_{\text{eff}} < 1.7$ are delocalized modes. These are produced by evanescent waves emitted by the dipole, and their contribution to the total radiated power is about 40%. The peaks in the dipole power spectrum with $1.7 < n_{\text{eff}} < 2.5$ are associated with guided modes and also induced by the dipole emission of evanescent waves. They carry slightly more than 45% of the total emission. The components with $n_{\text{eff}} > 2.5$ are purely evanescent and do not contribute in the radiative intensity.

For each reduced frequency, the measurement results covers all possible $k_{//}$ values in the light cone delimited by the air light line and seen clearly in this plot because no light can emit below the light line. Another characteristic line arises from the presence of the cutoff frequency for any given guided mode. This occurs when $k_{//}$ reaches the sapphire line, defined by $k_{//} = 1.7k_0$. For any given frequency, there is a

discrete number of guided modes carried by the planar cavity, with $1.7 < n_{\text{eff}} < 2.5$.

The lowest order mode has $n_{\text{eff}} < 2.5$. This mode almost perfectly follows the GaN

line, defined by $k_{//} = 2.5k_0$. The number of guided modes as measured with this

sample is in accordance with the simulation shown in previous Fig. 1B. To explain all

of the effects caused by a 2-D PhC particular in the effects related to polarization, the

field, associated with a guided modes for example, should be described as a Bloch

mode: $\mathbf{E}(\mathbf{r}) = \Sigma_{\mathbf{G}} \mathbf{E}_{\mathbf{G}} * \exp [i (k_{//} + \mathbf{G}) \cdot \mathbf{r}]$, where $\mathbf{E}_{\mathbf{G}}$ is the electric field component

corresponding to harmonic $\mathbf{G}$, and $k_{//}$ is the in-plane wave vector of the Bloch mode.

With our PhC structure, the reciprocal lattice (RL) in K space is a 2-D triangular

lattice rotated by 30° with respect to the direct lattice (DL) in real space and RL

vectors can be written as: $\mathbf{G} = h\mathbf{a}_1^* + k\mathbf{a}_2^*$, where h and k are integers, and $\mathbf{a}_1^*$ and $\mathbf{a}_2^*$

are the two RL basis vectors. Harmonics of the Bloch mode are extracted if their

in-plane wave vectors are within the light cone: $|k_{//} + \mathbf{G}| < k_0$. The most striking

feature observed in Figure 2-7(a) is the detection of the radiative components of

guided modes. The sets of lines labeled 2a and 2b are induced by the radiative

harmonics of the TE-polarized guided modes propagating in the $\mathit{\Gamma M}$ direction with

in-plane wave vectors $k_{//} + \mathbf{G}_{10}$ and $k_{//} + \mathbf{G}_{-10}$ (shown in Figure 2-7(b)), where shown

only a radiative harmonic associated with set 2b, for clarity; 2a is obtained by

symmetry. The sets of lines labeled 3a and 3b are formed by the combination of two

harmonics (as shown in Figure 2-8 for a line associated with set 3a). These radiative harmonics are not associated with guided modes propagating in the ΓM direction but in directions about $\pm 60°$. The measurement of these components constitutes direct evidence of 2-D PhC-assisted light extraction [12].
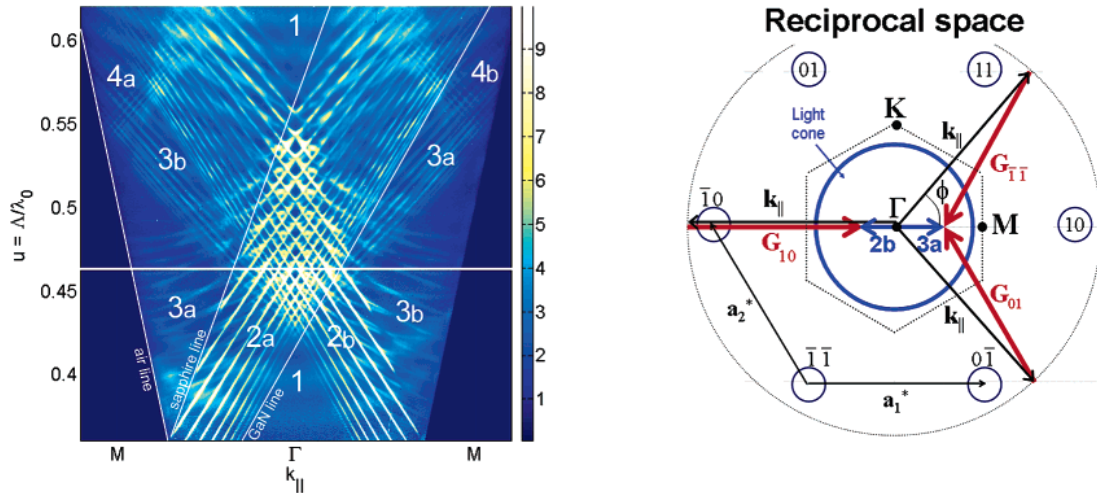
Figure 2-7(a) Normalized far-field PL spectrum of the PhC-assisted QD structure; (b) Reciprocal lattice associated with the 2-D PhC and origin of extracted guided modes. The blue and gray circles indicate the light cone and the trace of points with identical $k_{//}$, respectively. The gray hexagon is the first Brillouin zone boundary.
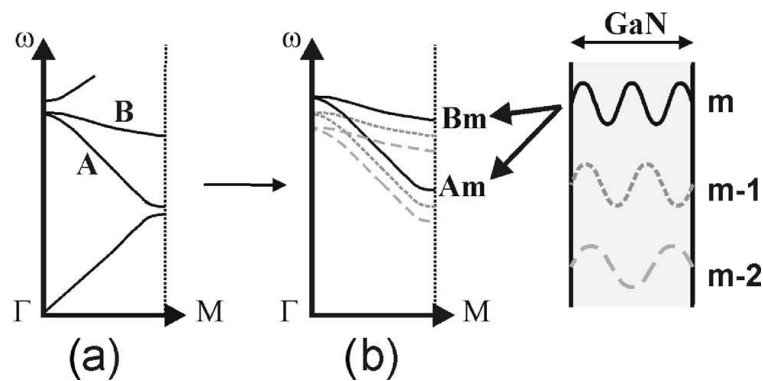
Figure 2-8(a) 2-D band structure of a PhC in the ΓM direction; (b) Corresponding band structure in a multimode waveguide: mode *m* gives rise to two PhC bands, *Am* and *Bm*.

References

[1] M. Imada, S. Noda, A. Chutinan, T. Tokuda, M. Murata, and G. Sasaki, *Appl. Phys .Lett.* **75**, 316 (1999)

[2] S. Noda, M. Yokoyama, M. Imada, A. Chutinan, and M. Mochizuki, *Science* **293**, 1123 (2001)

[3] H. Y. Ryu, S. H. Kwon, Y. J. Lee, and J. S. Kim, *Appl. Phys. Lett.* **80**, 3467 (2002)

[4] G. A. Turnbull, P. Andrew, W. L. Barns, and I. D. W. Samuel, *Appl. Phys. Lett.* **82**, 313 (2003)

[5] K. Sakai, E. Miyai, T. Sakaguchi, D. Ohnishi, T. Okano, and S. Noda, *IEEE J. Sel. Areas Commun.* 23, 1335-1340 (2005)

[6] M. Imada, A. Chutinan, S. Noda and M. Mochizuki *Phys. Rev. B* **65**, 195306 1-8 (2002)

[7] M. Yokoyama and S. Noda *Opt. Express* **13**, 2869-2880 (2005)

[8] M. Imada, A. Chutinan, S. Noda, M. Mochizuki, *Phy. Rev. B*, 65, 195306 (2002)

[9] M. Notomi, H. Suzuki, and T. Tamamura, *Appl. Phys. Lett.*, **78**, 1325 (2001)

[10] Fre ́de ́ric S. Diana, Aure ́lien David, Ines Meinel, Rajat Sharma, Claude Weisbuch, Shuji Nakamura and Pierre M. Petroff, *Nano Lett.*, Vol. **6**, 1116-1120 (2006)

[11] Soller, B. J.; Stuart, H. R.; Hall, D. G. *Opt. Lett.*, **26**, 18, 1421 (2001)

[12] A. David, C. Meier, R. Sharma, F. S. Diana, S. P. DenBaars, E. Hu, S. Nakamura,

C. Weisbuch, H. Benisty, *Appl. Phys. Lett.*, **87**, 101107 (2005)

Chapter 3

Fabrication of Nitride-based 2-D Photonic Crystal Surface Emitting Lasers

Introduction

Recently, photonic crystal (PhC), which are periodic patterns with sizes of nano-scale, are usually fabricated by lithography including E-beam lithography, holograph lithography, and nanoimprint lithography. However, holograph lithography has the limitation of the PhC pattern including PhC lattice constant and radius of PhC hole. The nano imprint lithograph has the difficult to fabricate the PhC imprint mask and lift-off PR/PMMA film from the sample. Therefore, the most popular method to fabricate the PhC pattern is by the E-beam lithography method because of the cheaper instrument and high resolution.

3-1 Electron-Beam Lithography System (EBL)

The first EBL machine, based on the scanning electron microscope (SEM), was developed in the 1960s. The technique of EBL is using electron beam to generate patterns on a surface and the De-Broglie relationship (λ <0.1nm for 10-50keV electrons) to avoid the diffraction limit. Therefore, we can overcome the diffraction

limit of light and create nano-scale pattern without mask by using this technique. The

EBL system usually consists of an electron gun for generating electron beam, a beam

blanker for controlling the electron beam, electron lens (objective lens) for focusing

the electron beam, a stage, and a computer with a controller system as shown in

Figure 3-1.
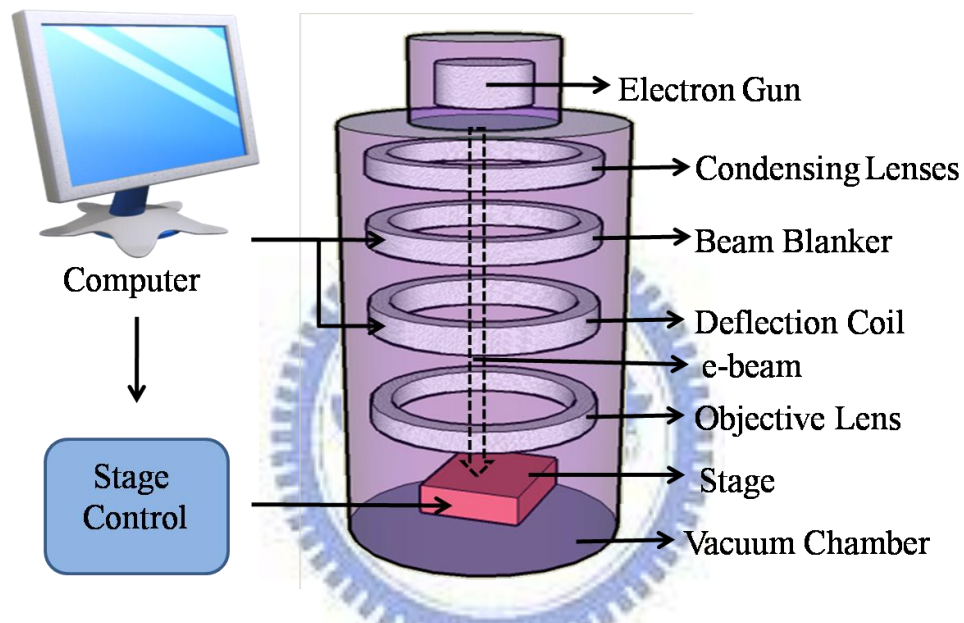
Figure 3.1 The typical schematic diagram of EBL system.

Electron sources

Electrons can be emitted from a conductor either by heating the conductor with a

sharp point where the electrons obtain sufficient energy from the thermal source to

overcome the work function of the conductor (thermal emission sources) or by

applying a strong electric field where the electrons can tunnel through the work

function (field emission sources). There are three key parameters of the electron

source such as actual spot size on sample, brightness and wide range energy of the

electrons. The actual spot size is determined by the number of the lenses; brightness is

similar to the intensity of light which can be controlled by the higher current in the

electron source.

Table 3-1 shows different types of electron sources. For our system, we use

"Thermal (Schottky) Field Emitter" as electron source. It combines a field emission

source with sharp tungsten and the heating of the thermal source. Due to the source tip

operation at 1800K, it is less sensitive to environmental gases and can achieve stable

operation for months.

Sources	Spot size (μ m)	Brightness (A/cm2/sr)	Vacuum requirement (Torr)
Tungsten Thermionic	25	~10^5	10^{-6}
Thermal (Schottky) Field Emitter	20	~10^8	10^{-9}
Cold Field Emitter	5	~10^9	10^{-10}

**Table 3-1 The properties of electron sources.**

Electron lenses

Since the electronic or magnetic field can control the electron beam path, we

called them "electron lenses". Although we can imagine electron lenses as optical

lenses, the electron lenses have shortage in ability of aberrations calibration,

especially in spherical aberration and chromatic aberration. To minimize the influence

caused by aberration, the electron beam should always confine at the center of lenses.

Beam blanker

The function of beam blanker can turn on or turn off the electron beam by

applied a electric filed. It usually consists of a pairs of plates as an electronic deflector.

Either or both plates are linked to a blanking amplifier with a fast response time. The

voltage is applied across the plates to turn the beam off. This function is necessary for

moving the beam from one designed structure to another with no leaky electron beam

current.
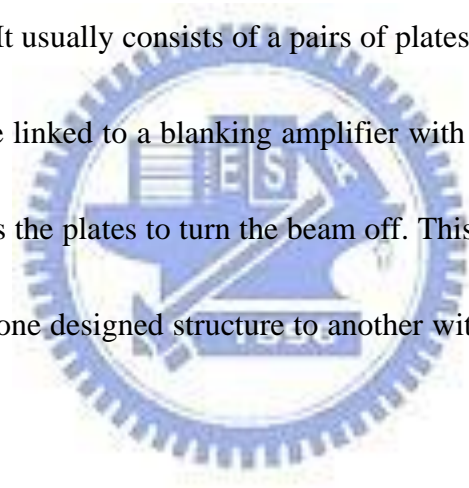
Stage and computer control system

The stage provides high resolution movement of sample and we use the computer

control system to dominate the movement of stage. Besides, the computer control

system can design the e-beam lithography pattern by GDS software.

3-2 Wafer Preparation

The GaN-based heterostructure of MCLED was grown by metal-organic chemical vapor deposition (MOCVD) system (EMCORE D-75) on the polished optical-grade c-face (0001) 2'' diameter sapphire substrate, as shown in Figure 3-2. Trimethylindium (TMIn), Trimethylgallium (TMGa), Trimethylaluminum (TMAl), and ammonia (NH_3) were used as the In, Ga, Al, and N sources, respectively. Initially, a thermal cleaning process was carried out at 1080°C for 10 minutes in a stream of hydrogen ambient before the growth of epitaxial layers to clean the sample surface. Second, the 30nm thick GaN nucleation layer was first grown on the sapphire substrate at 530°C, and then 2µm thick undoped GaN buffer layer was grown on it at 1040°C. After that, a 35 pairs of quarter-wave GaN/AlN structure was grown at 1040°C under the fixed chamber pressure of 100Torr and used as the high reflectivity bottom DBR. Finally, the 5λ active pn-junction region was grown atop the GaN/AlN DBR, composed typically of ten pairs $In_{0.2}Ga_{0.8}N$ quantum wells (L_W=2.5 nm) with GaN barriers (L_B=7.5 nm), surrounded by 560nm thick Si-doped n-type GaN layer, and 200nm thick Mg-doped p-type GaN layers. The reflectivity spectrum of the half structure with 35 pairs of GaN/AlN DBR structure was measured by the n&k ultraviolet-visible spectrometer with normal incident at room temperature, as shown in Figure 3-3. The reflectivity spectrum centered at 430nm and stopband width of about 28nm.
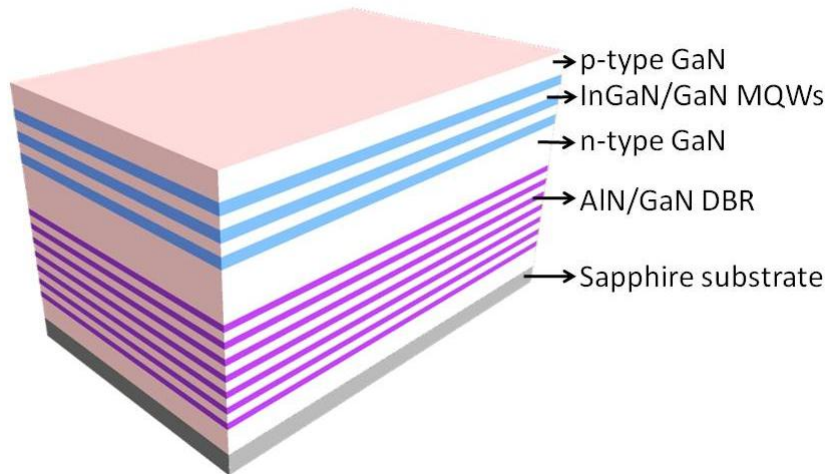
Figure 3-2 The 2-D schematic diagram of nitride structure grown by MOCVD.
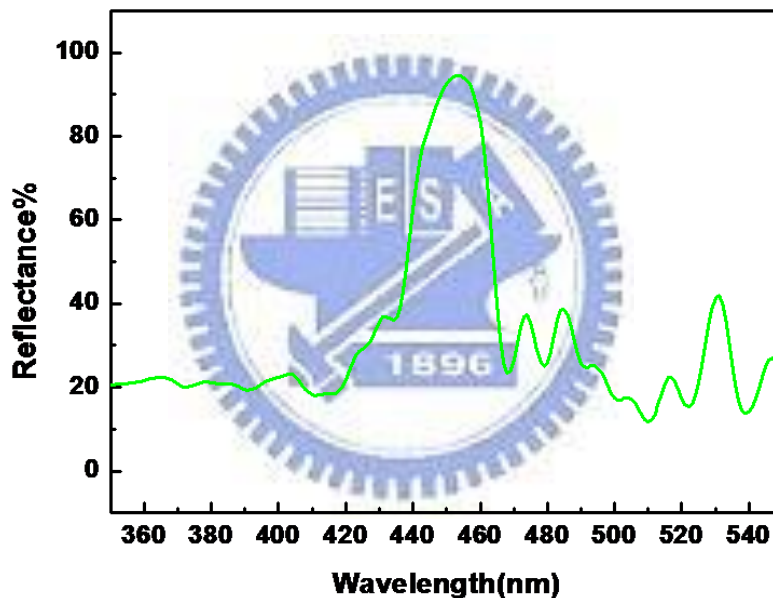

Figure 3-3 Reflectivity spectrum of the half structure with 25 pairs of GaN/AlN DBR structure measured by n&k ultraviolet-visible spectrometer with normal incident at room temperature.

3-3 Process Procedure

There are some principles to fabricate GaN-based PCSELs, including initial clean (I.C.), plasma enhanced chemical vapour deposition (PECVD) technique, EBL technique, and inductively coupled plasma - reactive ion etching (ICP-RIE) technique.

The purpose of the I.C. is to remove the small particle and organism on the sample surface. The steps of I.C. are described as below.

Initial Clean (I.C.)

1. Degreasing particles in acetone (ACE) 5min by ultrasonic baths.

2. Dipping in isopropyl alcohol (IPA) 5min by ultrasonic baths for organism removed.

3. Rising in de-ionized water (D.I. water) 5min for surface clean.

4. Blowing with N_2 gas for surface drying.

5. Baking by hot plate 120^oC, 5min, for wafer drying.

PECVD (SAMCO PD220)

The purpose of PECVD technique is to deposit a SiN_x film for hard mask. The details of PECVD parameters are expressed as below.

1. Initial clean

2. SiN_x film deposition :

   $SiHl_4$/Ar: 20sccm

   NH_3: 10sccm
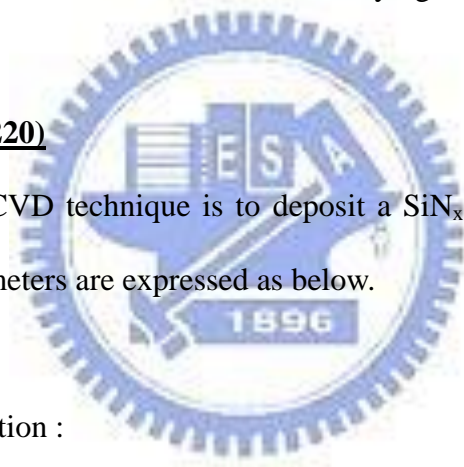
   N_2: 490sccm

   Temperature: 300℃

   RF power: 35W

   Pressure: 100Pa

   Time: 20min for depositing SiN_x 200nm

EBL

The purpose of the EBL is to define the PhC pattern on the photoresist (PMMA) (soft mask). In the process of EBL, a special positive photoresist PMMA (A3) was used. These EBL parameters are described as below.

1. Spin coating use the photoresist: PMMA (A3).

    a. First step: 1000 rpm for 10sec.

    b. Second step: 5000 rpm for 90sec.

2. Hard bake: hot plate $180^{\circ}C$, 1hr.

3. Exposure :
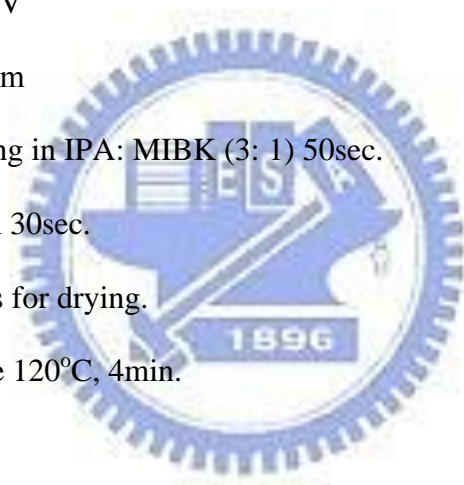
    Beam voltage: 10KeV

    Write field size: 50μm

4. Development: dipping in IPA: MIBK (3: 1) 50sec.

5. Fixing: rising in IPA 30sec.

6. Blowing with N_2 gas for drying.

7. Hard bake : hot plate $120^{\circ}C$, 4min.

ICP-RIE (Oxford Plasmalab system 100)

The soft mask was transfered to SiN_x film to form the hard mask by using ICP-RIE. These ICP-RIE techniques are described as below.

1. SiN_x film etching:

    Ar/O_2: 5sccm

    CHF_3: 50sccm

    Forward power: 150W

    Pressure: $7.5*10^{-9}$Torr

    Temperature: 20℃

Time: 100 second for etching SiN_x film 200nm

2. Initial clean for remove soft mask

ICP-RIE (SAMCO RIE-101PH)

The purpose of the ICP-RIE techique is to form the PhC layer on GaN. The hard mask was transferred to GaN by using ICP-RIE techique. Figure 3-4 are shown the SEM image of top view and cross section of completed 2-D PCSELs, respectively. These ICP-RIE techniques are described as below.

1. P-GaN etching:

  Ar: 10sccm

  Cl_2: 25sccm

  ICP power: 200W

  Bias power: 200W

  Pressure: 0.33Pa

2. Dipping BOE 40sec. for remove hard mask
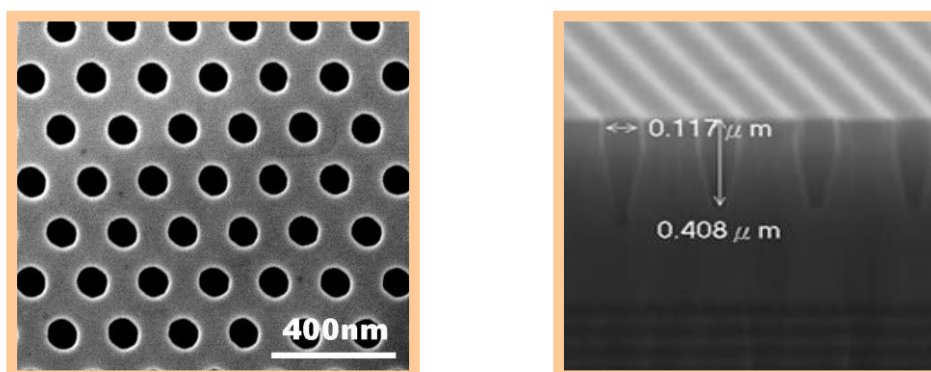
3. Polishing sapphire for optical pumping

Figure 3-4 SEM images of plane view and cross section of PhC pattern.
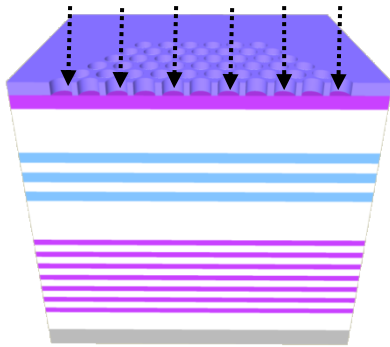
3-4 Process flowcharts

The PCSELs was fabricated by following process steps. In the beginning, the hard mask SiN_x 200nm was deposited by PECVD. Then PMMA layer (150nm) was spun by spinner and exposed using E-beam writer to form soft mask. The pattern on soft mask was transferred to SiN_x film to form the hard mask by using ICP-RIE (Oxford Plasmalab system 100), and then the PMMA layer was removed by dipping ACE. The pattern on hard mask was transferred to GaN by using ICP-RIE (SAMCO RIE-101PH) to form the PC layer. Finally, the sample dips in BOE to remove the hard mask.

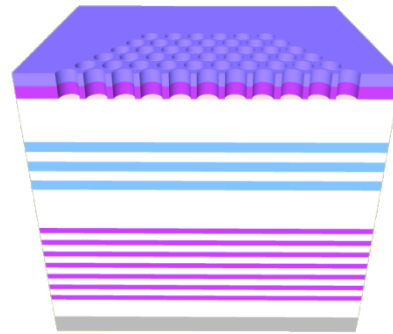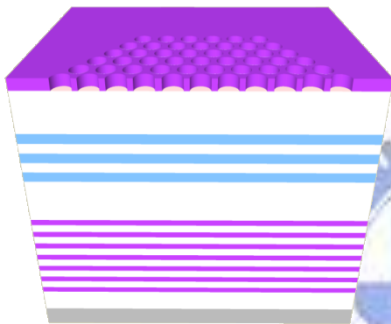**(a) SiN_x film**   **(b) PMMA**

(c) E-beam writing & developing

(d) Mask transfer by ICP-RIE

(e) Remove PMMA by acetone
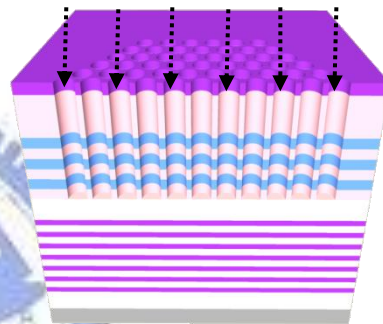
(f) ICP dry etching

Figure 3-5 Process flowchart of PCSELs, steps are ordered from (a) to (f).

p-type GaN

InGaN/GaN MQWs

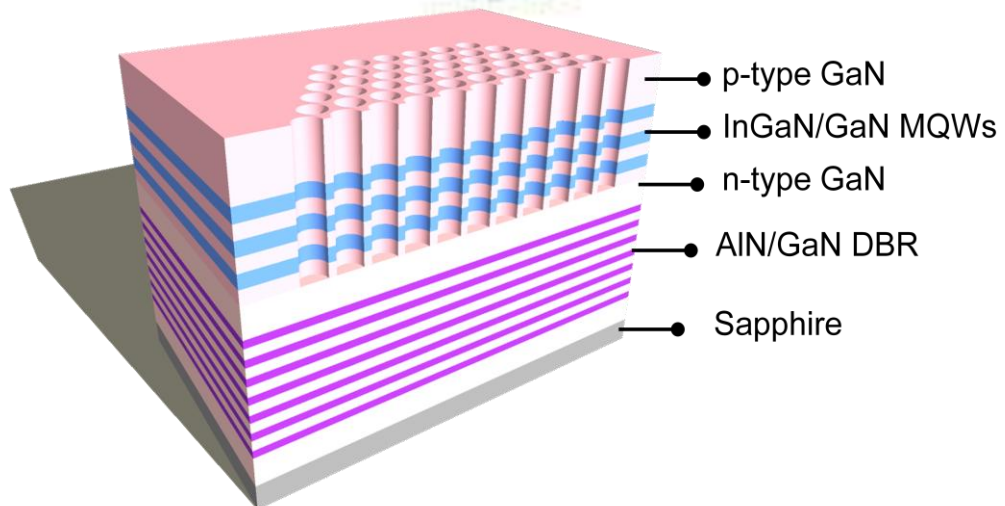n-type GaN

AlN/GaN DBR

Sapphire

Figure 3-6 Complete PCSELs' device after removing SiN$_x$ film.

To completely describe the process flowchart, each process conditions are entirely

listed in the Table 3-2.

| Step	Process	Conditions
1	Soft mask	Initial clean(I.C.) (2) Deposit 200nm SiN$_x$ by PECVD. (3) Spin 150nm PMMA by spinner. (4) Define PCSELs pattern by EBL. (5) Development. (6) Hard bake
2	Hard mask	(1) Dry etching by ICP-RIE (Oxford Plasmalab system 100) to form the hard mask. (2) Remove PMMA by ACE. (3) Hard bake.
3	PCSELs	(1) Dry etching by ICP-RIE ((SAMCO RIE-101PH) to transfer the hard mask to GaN. (2) Remove hard mask by BOE. (3) Hard bake.

Table 3-2 Detailed process flowchart of PCSELs.

3-5 The design for PCSELs

In this section, we focus on the design for our GaN-based 2-D PCSELs. Initially, we calculate the TE-like mode dispersion band diagram to determine the normalized frequency which we choose for specific band-edge groups. Normalized frequency is the ratio of the lasing wavelengths of optical modes and the PhC lattice constants. Once the lasing wavelength is determined, the lattice constant is certain to be determined. The lasing wavelength is located within the emission of the active layer. According to the theory described in chapter 2, the surface emitting laser in the photonic crystal grating structure could only happen as the Bragg condition is satisfied. In additional, the Bragg condition is satisfied at Brillouin zone boundary including Γ, K and M points. At these points, light waves have opportunity to diffract normally to the sample surface which was described in section 2.2. Therefore, we can design a GaN-based 2-D PCSEL operating at the designed lasing wavelength with the optimized PhC lattice constant at Brillouin zone boundary, Γ, K and M point, which can be defined in the photonic band diagram.

In this study, we fix the parameter, r/a, to be 0.28 for calculating the band diagram of PhC using 2-D plan wave expansion method (PWEM). In fact, the 2-D PWEM couldn't precisely evaluate the photonic band diagram of our 3-D structure. That means we should do some modification to parameters describing our structure and

then bring them into the 2-D PWEM to approximate real condition. Therefore, according to reference [1], we further bring two parameters including confinement factor (Γ_g) and effective refractive index (n_{eff}) into our calculation. Γ_g is the ratio of the light field confined within the 2-D PhC structure to the light inside the whole device, and n_{eff} is the effective refractive index of the entire device with PhC that take into account the effects of partial modal overlap of electromagnetic fields. Γ_g and n_{eff} could be used to estimate the effective dielectric constant of nano-hole (ε_a) and the background (ε_b) for 2-D PWEM calculation to further approximate the 3-D structure. These two parameters can be obtained by solving the distribution of the electric field in the in-plane direction. The Γ_g and n_{eff} for describing our structure are estimated to be 0.563 and 2.495 considering fundamental mode, respectively. It is first estimated by transfer matrix method and shown in Figure 3-7.
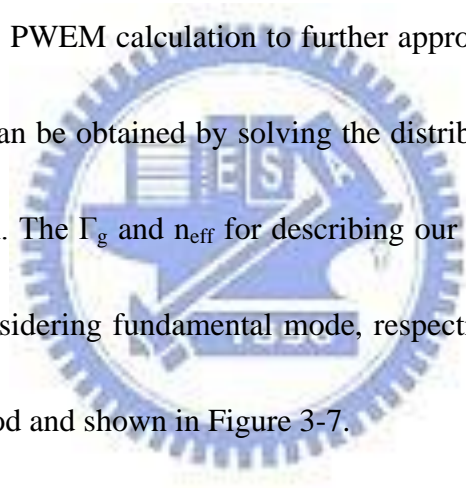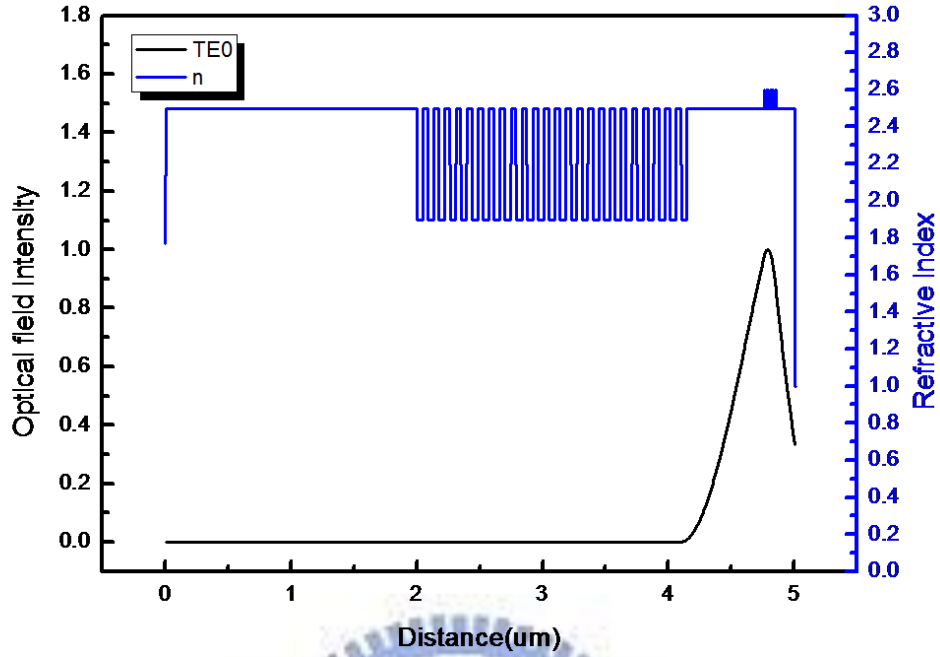
Figure 3-7 The lowest guided mode optical field distribution, where the confinement factor Γ=0.9284 and n_eff=2.4981.

Then, we could determine ε_a and ε_b using two conditions:

$$n_{eff}^{\,2} = f\varepsilon_a + (1-f)\varepsilon_b$$ (3.1)

$$\Delta\varepsilon = \varepsilon_b - \varepsilon_a = \Gamma_g\left(\varepsilon_{mat} - \varepsilon_{air}\right)$$ (3.2)

where the f is a filling factor, ε_{mat} is the dielectric constant of semiconductor, and ε_{air} is the dielectric constant of air. For a triangular lattice PhC, f is written as:

$$f = \frac{2\pi r^2}{\sqrt{3}a^2}$$ (3.3)

Therefore, the value of ε_a and ε_b in unit cell for our PhC device could be obtained the values of about 4.11 and 7.07, respectively. To bring ε_a and ε_b into the calculation, a band diagram of the 2-D PhC structure with triangular lattice for TE-like mode with

r/a=0.28 on our sample structure could be estimated as shown in Fig 3-8. The figure shows that the dispersion curve of each mode would cross and splits at specific band-edges, and the mode density is higher at those boundaries. Light at these areas can propagate along different direction and have chance to couple and form a laser cavity. According to the theory described in chapter 2, the surface emitting behavior in the photonic crystal grating structure could only happen when the Bragg condition is satisfied.
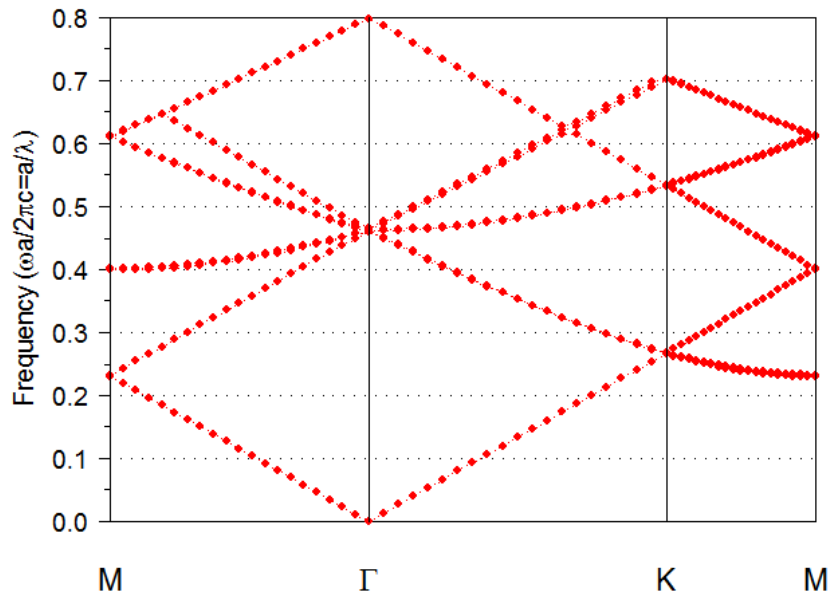

Figure 3-8 The TE band dispersion diagram of our design.

In order to get a high opportunity of those band edge modes satisfying Bragg condition, the lattice constant of photonic crystal were determined between 190nm and 300nm correspond to the normalized frequency ranging from 0.45 to 0.7, considering a PL peak wavelength ranging from 460nm to 420nm, and pumped by

YVO4 laser (laser wavelength=355nm) and HeCd laser (laser wavelength=325nm) as

shown in Fig. 3-9, respectively. The photoluminescence of the sample used in this

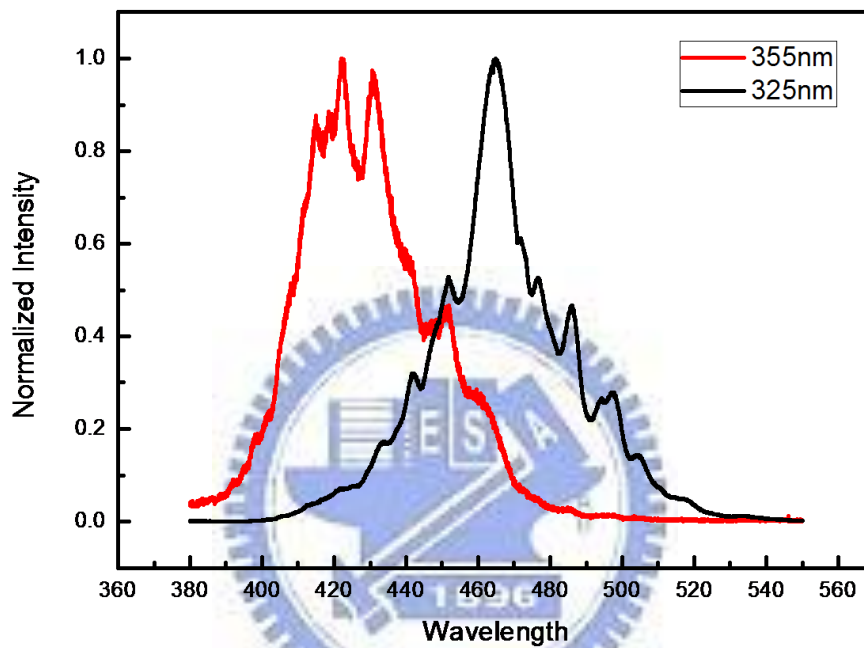experiment was centered at around 425 nm.

Figure 3-9 The μ-PL spectrum of as-grown sample was pumped by YVO4 laser (laser wavelength=355nm) and HeCd laser (laser wavelength=325nm), respectively.

Chapter 4

Optical Characteristics of GaN-based 2D Photonic Crystal Surface Emitting Lasers

4-1 Optical pumping system (Angle-resolved μ-PL)

The angle-resolved μ-PL (AR μ-PL) system is designed for multiple choices. As shown in Figure 4-1, we have two optical pump sources, two optical pump incidence paths, two collecting PL method and two way to collect sample surface image. The two optical pump sources are: one is frequency tripled Nd:YVO$_4$ 355nm pulsed laser with a pulse width of ~0.5ns at a repetition rate of 1KHz; the other is 325 nm HeCd continuous wavelength laser. The samples are optically pumped by laser beam with an incident angle of 0° or 60° to the sample. The laser spot size is about 50μm in diameter so that covering the whole PhCs pattern area. The PL is collected by a 15X objective lens and straightly collected by spectrometer with a charge-coupled device (Jobin-Yvon IHR320 Spectrometer) or collected by a fiber with a 600μm core, which rotating in the normal plane of the sample, and also coupled into spectrometer. The spectral resolution is about 0.07nm for spectral output measurement. Figure 4-1 shows the setup of our AR μ-PL system. The GaN-based PCSELs were placed in a cryogenics controlled chamber for performing PL experiment under low temperature

(in order to prevent damage caused by heat). The temperature of the chamber can be

controlled from room temperature (300K) down to 77K via the liquid nitrogen. We

can also monitor the image and spatial distribution on the sample surface by

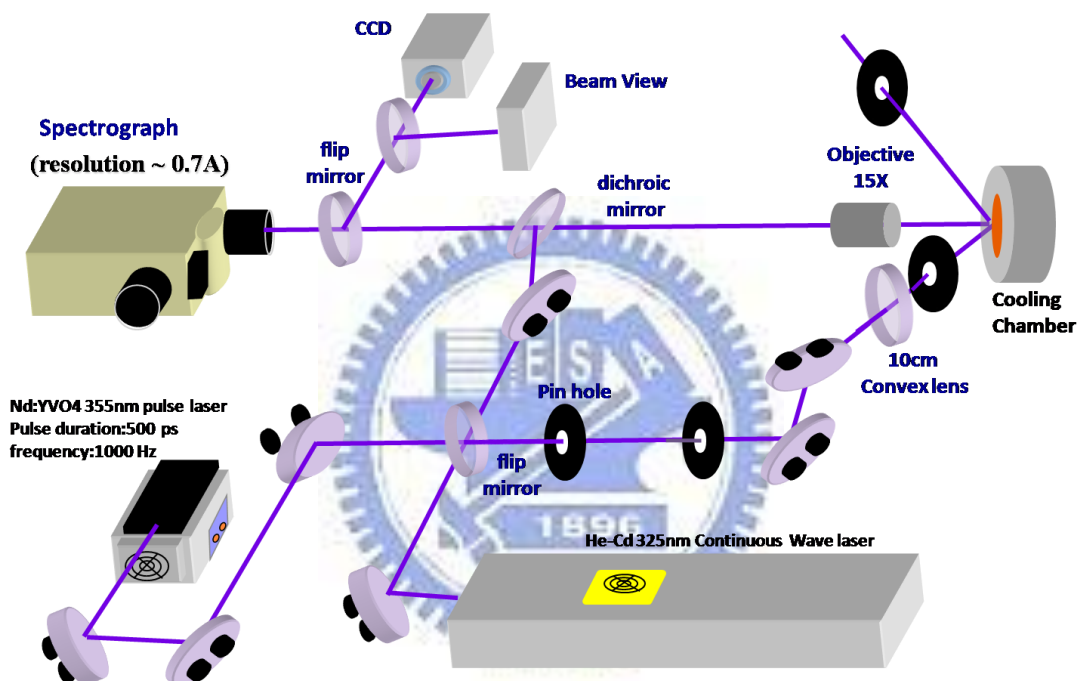charge-coupled device (CCD) and beam view, respectively.

Figure 4-1 The angle-resolved μ-PL (AR μ-PL) system.

4-2 Data normalization

We set up a rotational stage just under the sample stage to measure the light field

distribution which emitted by PCSELs. In this way, the rotation center would match

the sample center roughly. We have a detected arm connected the rotational stage and

the fiber detector. Rotating the rotational stage, the fiber could collect PL spectrum at

different angle. Therefore, we have a series of PL spectra distributed in continuous

space, we named these spectra as "angle-resolved μ-PL" (AR μ-PL).

After measurements, we transformed the AR μ-PL spectra to obtain the guided

modes dispersion relationships (reduced frequency $u=\Lambda/\lambda_0$ as y-axis versus in-plane

wave vector, $k//$, as x-axis), by using the relation $k// = k_0 \sin\theta$. In addition, for each

wavelength, $I_{PL}(\tilde{o})$ is normalized relative to its integrated intensity[1]. The resulting

normalized AR μ-PL diagram, shown in Figure 4-1(b), reveals the dispersion

relationships of guided modes and points to details about their relative excitation and
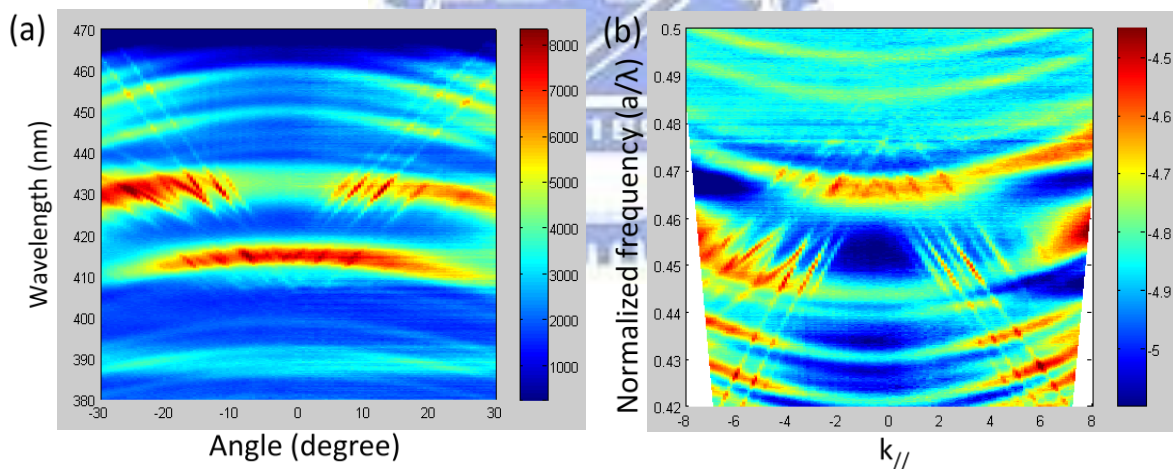
out-coupling efficiency.

Figure 4-2 The AR μ-PL diagrams (a)before and (b)after normalization where the colorbar represents intensity and relative intensity with log value, respectively.

4-3 Experimental results of different pairs of DBR

Our group has successfully demonstrated the PCSEL by using the nitride-based

"Distributed Bragg Reflector"(DBR) structure. The DBR has high reflectivity and low

refractive index layer to provide better confinement factor of light within the entire

structure. Figure 4-3 are the SEM and TEM images. From the SEM image, we can

observe the GaN cavity and AlN/GaN DBR. In the TEM image, we can observe

clearly the insertion of GaN superlattice layer in the DBR structure. The insertion of

superlattice layer can relax strain so that we can achieve high reflectivity of
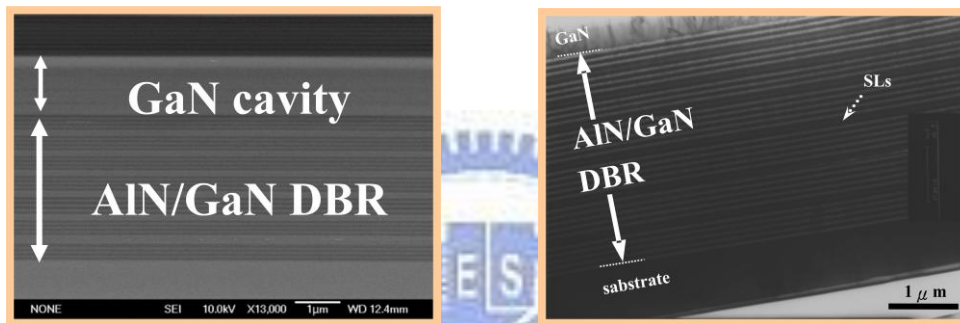
nitride-based DBR [2,3].

Figure 4-3 (a)SEM; (b)TEM image of DBR structure.

In order to differentiate the influence caused by DBR from the diffraction pattern

caused by PhCs, we measured AR μ-PL diagrams for two structures: the first type is

25 pairs of DBR structure, which is our normal design for PCSELs; the second type is

5 pairs of DBR, which has lower ability of light field confinement. We simulated the

fundamental guided mode by waveguide theory in different DBR pairs structures. Due

to the variation of thickness of low refractive index, there is a huge partial of light

field is distributed outside the cavity region (or we called it "leaky") when the DBR

pairs is below 25, shown in Figure 4-4(a).

Further, we also simulated light field distributions for higher order guided modes.

Figure 4-4(b) show the confinement factor, which is the light field confined in the

PhCs region over the light field in the entire structure, versus guided modes in

different pairs of DBR. It's clear that the confinement factor has increased obviously

at 25 pairs of DBR. Therefore, the standard structure of PCSELs is fabricated with 25
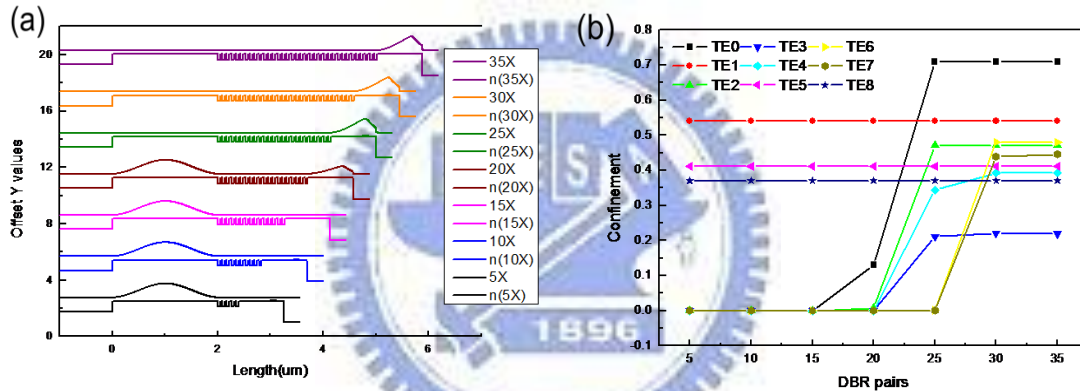
pairs of DBR pairs.

Figure 4-4 (a)The light field distribution of fundamental guided mode (TE0)；(b)The

confinement factor of guided modes in different pairs numbers of DBR structure.

It is worth to notice that the two PhCs patterns of 5 and 25 DBR pairs structure

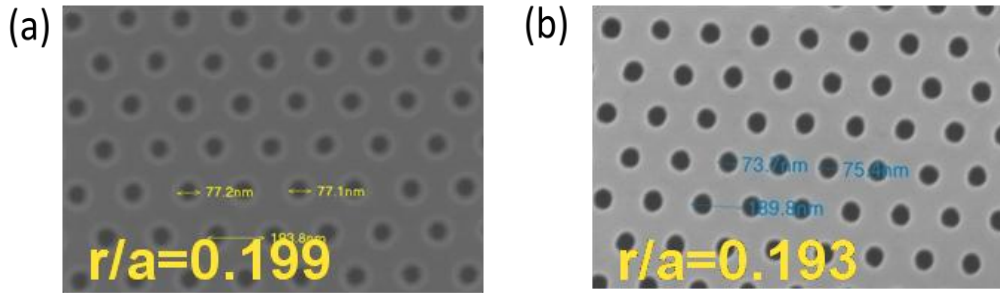own the same r/a ratio(shown in Figure 4-5) which represent they own the same PCs'

characteristics.

Figure 4-5 The SEM images of (a)25 pairs DBR; (b)5 pairs DBR which shows the same r/a ratio.

Figure 4-6 is the AR μ-PL diagrams of 25 and 5 pairs DBR(left and right diagram, respectively) where two kinds of modes are observed: Fabry–Pérot modes (background broad curves), present in any planar structure with embedded MQWs and DBR structure, and guided modes diffracted by the PhCs (sharp lines) corresponding to an enhancement on the total emitted light due to the PhCs on the surface. Since those emitted light are guided modes coupled with band structure, these lines clearly clarify the characteristics of PhCs. We simulated the band structure by RSoft commercial software using the parameters of the exact PCSEL device we measured and mapped the band structure with the AR μ-PL diagram. Since the slope of diffraction lines in both AR μ-PL diagrams show good agreement with the same band structure, we can tell that the PhCs structures show the same slope of diffraction lines if they own the same characteristics(ex. r/a ratio). Although Figure 4-6 shown the same slope of diffraction lines, they shown different numbers of diffraction lines.

We simulated the guided modes (TE0 mode to TE8 mode, by waveguide theory) exhibited in both two structures which shown in Figure 4-7(a) and (b). The integral light field intensity in the PhCs structure is shown in Figure 4-7(c) and (d). From Figure 4-7(c) and (d), we observed 25 pairs DBR provided better confinement from 5 pairs DBR. That is also the reason why we can see more diffraction lines in 25 pairs DBR structure.
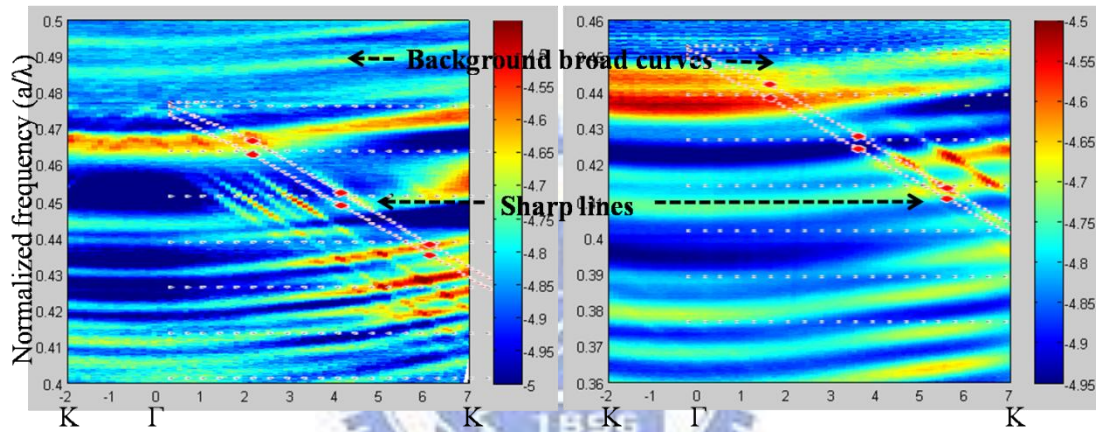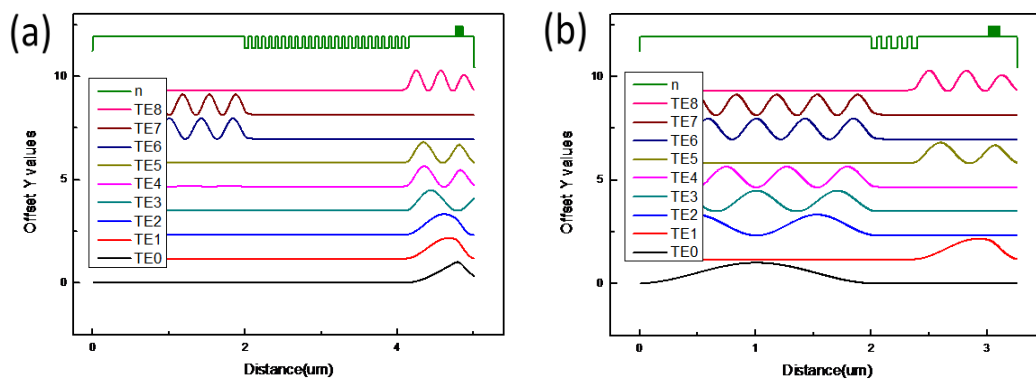

Figure 4-6 The angle-resolved μ-PL diagram (left diagram is for 25 pairs of DBR, right is for 5 pairs of DBR) shows two kinds of modes : Fabry–Pérot modes (background broad curves), present in any planar structure with embedded QWs, and guided modes diffracted by the PhCs (sharp lines).
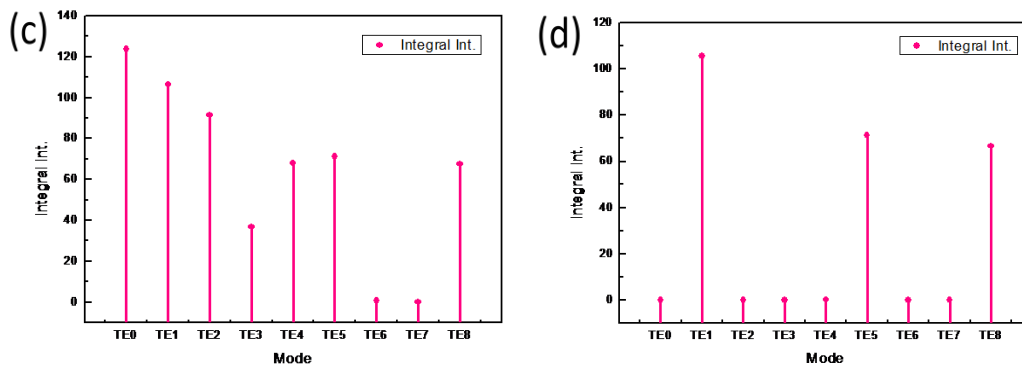
Figure 4-7 (a),(c)The guided mode profile in the entire structure and integral light field intensity within PhCs structure for 25 pairs DBR; (b),(d) are for 5 pairs DBR, respectively.

4-4 The lasing behavior of GaN-based 2D PCSELs

Previously, our group had measured three types of band-edge mode: Γ, K, M mode by fabricated a series of PCSEL. Compared with Figure 4-8(a) and (b), we can precisely coincided our experimental data with these three band-edge frequencies (Γ1, K2, M3) [4]. In this section, we investigated the lasing behavior and mechanism of three band-edge modes (Γ1, K2, M3) thoroughly.
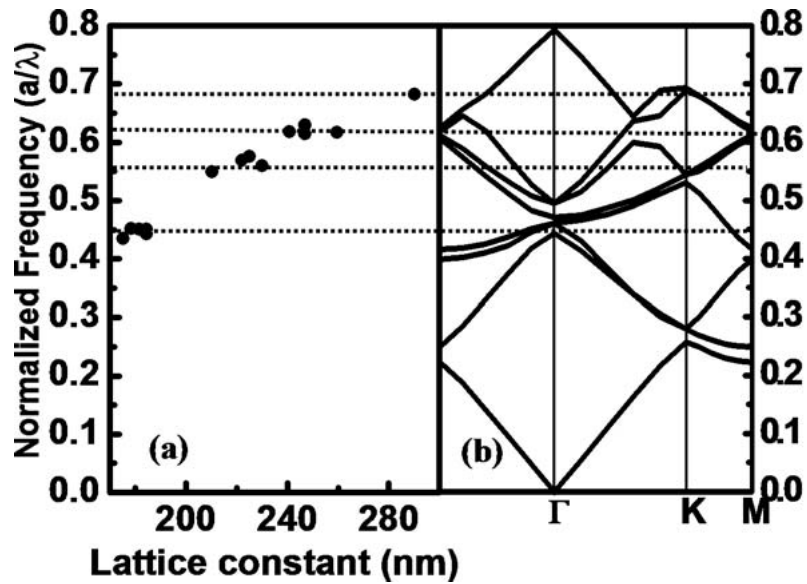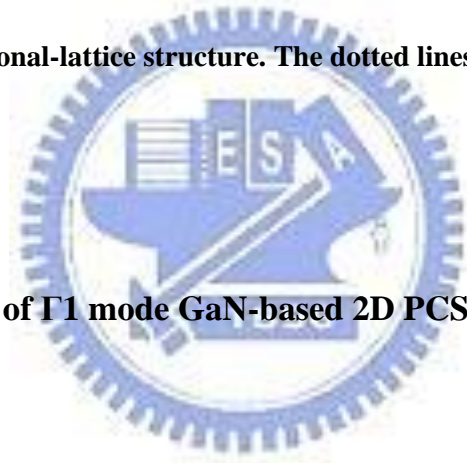
Figure 4-8 (a) Normalized frequency as a function of the lattice constant. The solid circle points are the lasing wavelengths from the different PC structures. (b) Calculated band diagram of the 2D hexagonal-lattice structure. The dotted lines are guides for band edges. [4]

4-4.1 Characteristics of Γ1 mode GaN-based 2D PCSELs

<u>Lasing action</u>

The PCSELs is fabricated by the standard process flowchart. The r/a ratio (where r is the radius of hole, a is lattice constant) of PhCs is 0.286. We optical pumped the PCSEL at 77K and the lasing spectrum is shown in Figure 4-10. Since the lattice constant (a) is 190nm, the a/λ ratio is 0.48. Due to the design for lasing action at Γ1 device which parameters are described as follows:

$$r/a=0.286, a=191nm, n_b= 2.603, n_a= 1.747, n_{eff}= 2.498$$

put these parameters in R-soft software and plot the band structure (dispersion

diagram) for TE-like mode as shown in Figure 4-9. The a/λ ratio observed by

experimental result is 0.48 which matched the Γ1 mode normalized frequency as

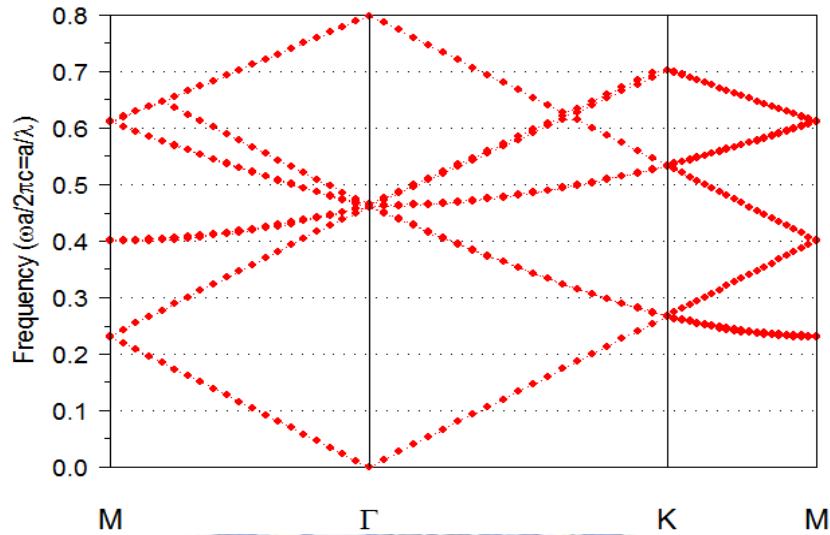shown in Figure 4-9. For this reason, we believed this PCSEL lasing at Γ1 mode.

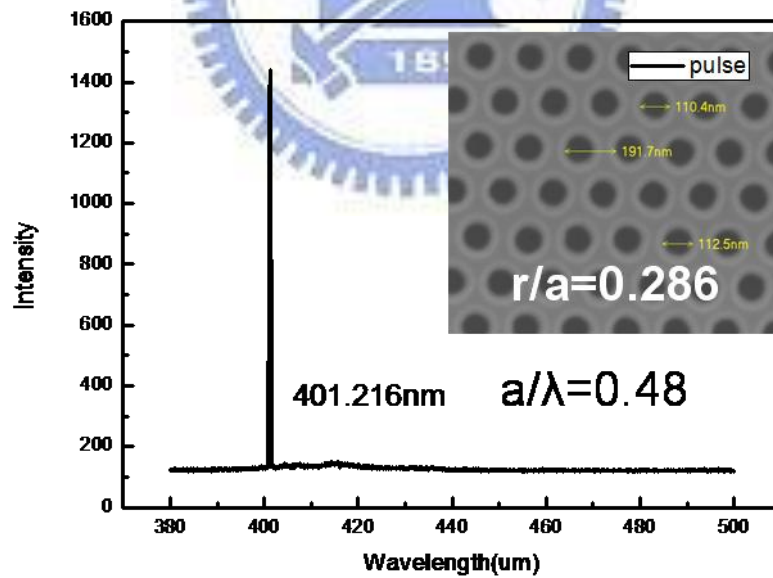**Figure 4-9 The band structure of Γ1 mode for TE-like mode.**

Figure 4-10 The PL spectrum under lasing action (inset: the SEM image of the PCSELs.

AR µ-PL diagram

To investigate whether our periodic structure possess the characteristics of PhCs,

we measured the photonic band diagram (or AR μ-PL diagram) by observing the resonant coupling of light from the active layer to the 2D GaN/air periodic structure. For a given frequency, resonant coupling occurs when the in-plane wave vector of light matches the wave vector of photonic bands. Therefore, we excited the device by using either YVO4 pulse laser or HeCd CW laser.

Figure 4-11 show the AR μ-PL diagram of Γ1 mode (Left: pumped by YVO4 pulse laser; right: pumped by HeCd laser) and the dot-dash line shows simulated band structure around Γ1 mode. In spontaneous emission diagram (right picture), the coupling can be observed as a sharp peak. The in-plane wave vector k is related to the polar angle θ by the relation: $k=(2\pi/\lambda)\sin\theta$. By varying the θ defined with respect to the direction normal to the plane and shifting the in-plane direction from Γ to both K and M direction, the photonic band can be mapped with simulated band structure around Γ point. We observed different slopes of diffraction lines in the photonic band. The diffraction lines with different slopes represent different band in the band diagram and we could mapped the band structure with photonic band precisely. Furthermore, we observed the PCSEL lasing at the second lowest mode, and we clearly measured the lower part of band structure. In Figure 4-13, the gain distribution for the four Γ1 mode, the lower two mode is in material, the other two is in hole[5]. Since our device is air hole structure, we only have gain in material, it is nature for us to measure the

lower band structure and lasing at the second lowest mode. By the way, the range of

spontaneous emission wavelength of our device is also in the lower part of band
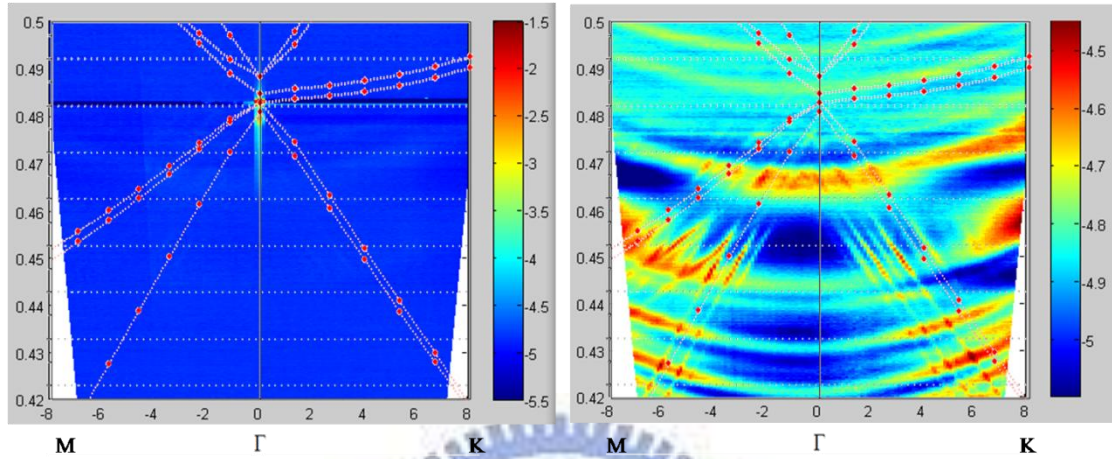
structure.

Figure 4-11 The AR µ-PL diagram of Γ1 mode (Left: pumped by YVO4 pulse laser;

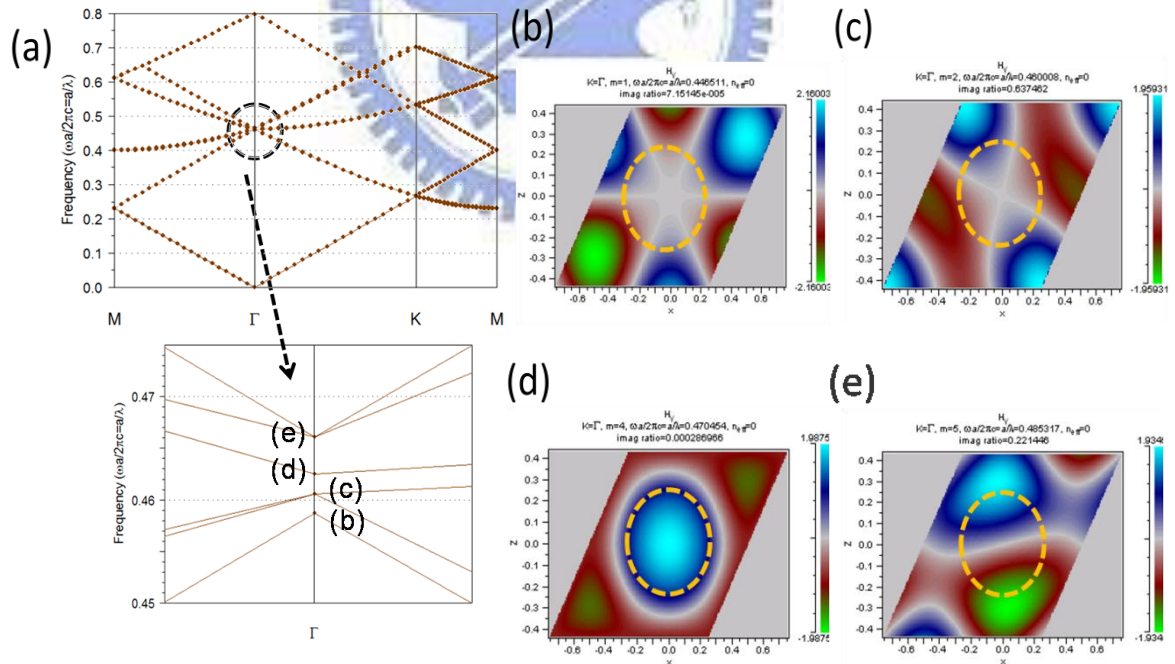**Right: pumped by HeCd laser), the dot-dash line shows band structure.**

Figure 4-13 (a)Upper: Complete band structure; Lower: The magnified band structure

around Γ1 mode. (b)-(e) are the magnetic field distributions of six modes in bands b-e.

Blue and green areas correspond to positive and negative magnetic fields perpendicular

to the plane. Orange circles indicate lattice points.

<u>Divergence angle & Polarization</u>

The divergence angle is shown in Figure 4-12(a). The maximum value of the lasing wavelength distribution is at zero degree and the divergence angle is about 1.2 degree which is much narrower than the VCSELs'. The polarization shown in Figure 4-12(b) is measured at the maximum peak and the degree of polarization (DOP) is about 33%. Since the guided mode also extracted by PhCs, the DOP is relatively low as a laser.
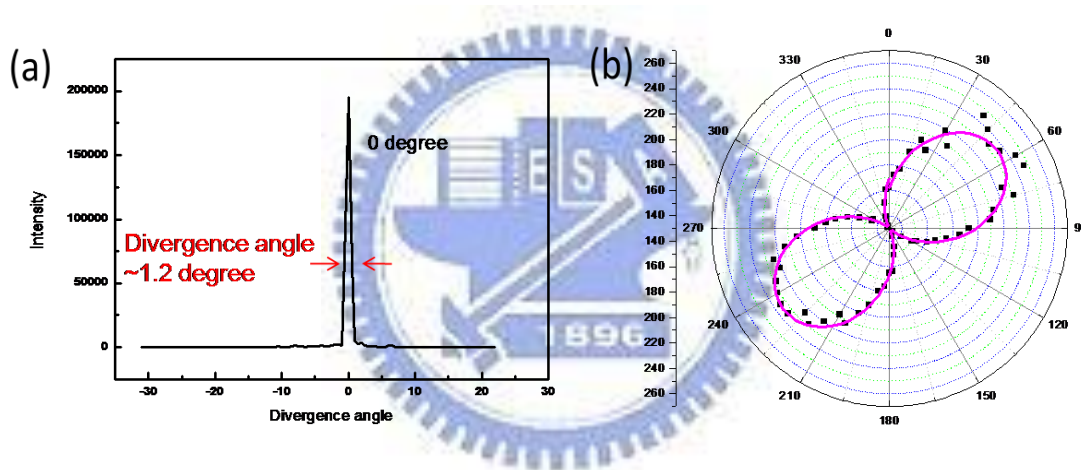

Figure 4-12 (a)The divergence angle on the normal plane; (b)The polarization measured at 0° of Γ1 mode.

<u>Far-field pattern</u>

The far-field pattern and divergence angle on normal plane shown in Figure 4-14. The far-field pattern is symmetric due to the symmetric structure of PhCs, and the divergence angle between two beams is about 5.7 degree.
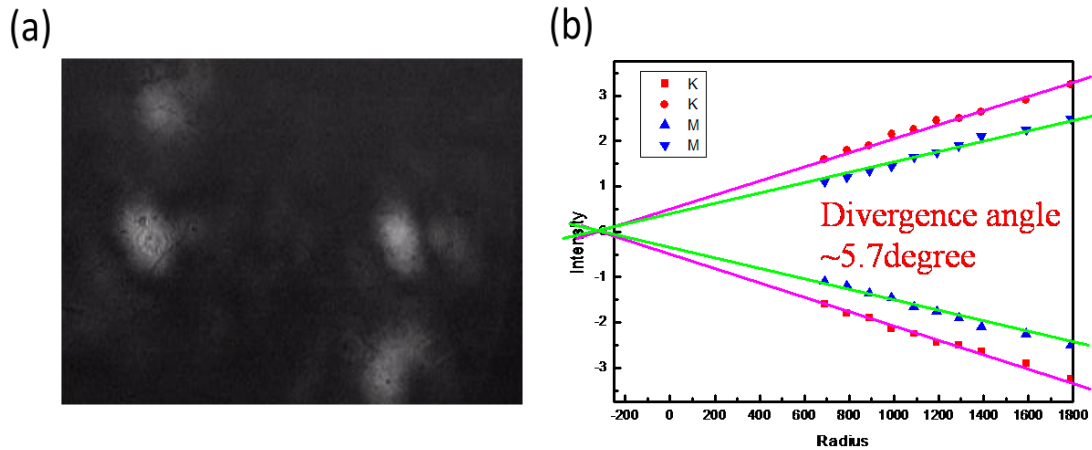
Figure 4-14 (a)The far field pattern collected by objective lens; (b)The divergence angle between the two beam.

4-4.2 Characteristics of K2 mode GaN-based 2D PCSELs

Lasing action

The r/a ratio (where r is the radius of hole, a is lattice constant) of PhCs is 0.286. We optical pumped the PCSEL at 77K and the lasing spectrum is shown in Figure 4-16. Since the lattice constant (a) is 230nm, the a/λ ratio is 0.56. Due to the design for lasing action at K2 device which parameters are described as follows:

$$r/a=0.285, a=230nm, n_b=2.560, n_a= 2.343, n_{eff}= 2.498$$

put these parameters in R-soft software and plot the band structure (dispersion diagram) for TE-like mode as shown in Figure 4-15. The a/λ ratio observed by experimental result is 0.56 which matched the K2 mode normalized frequency as shown in Figure 4-15. For this reason, we believed this PCSEL lasing at K2 mode.
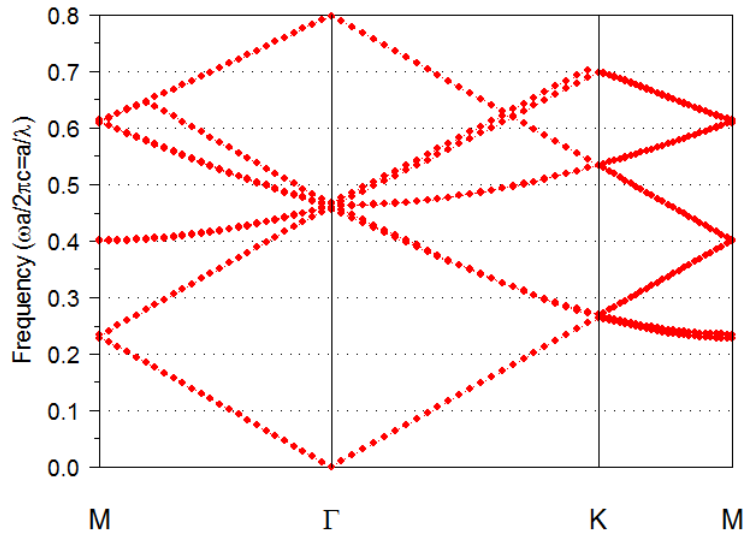
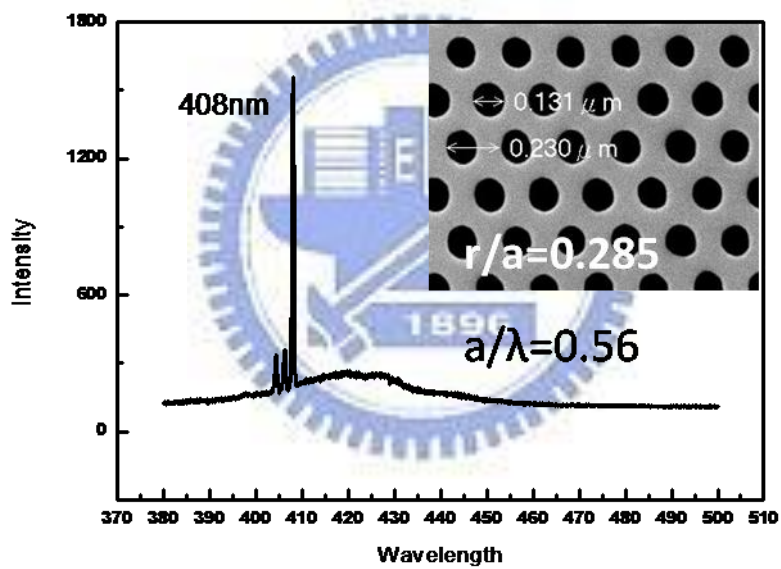**Figure 4-15 The band structure of K2 mode for TE-like mode.**

Figure 4-16 The PL spectrum under lasing action (inset: the SEM image of the PCSELs.

AR μ-PL diagram

Figure 4-17 show the AR μ-PL diagram of K2 mode (Left: pumped by YVO4

pulse laser; right: pumped by HeCd laser) and the dot-dash line shows simulated band

structure around K2 mode. By varying the θ defined with respect to the direction

normal to the plane and shifting the in-plane direction from Γ to K direction, the

photonic band can be mapped with simulated band structure around K point. We

observed one slope of diffraction lines in the photonic band. The diffraction lines

mapped with the band from Γ to K direction in the band diagram and we could

mapped the simulated band structure with photonic band precisely. Furthermore, we

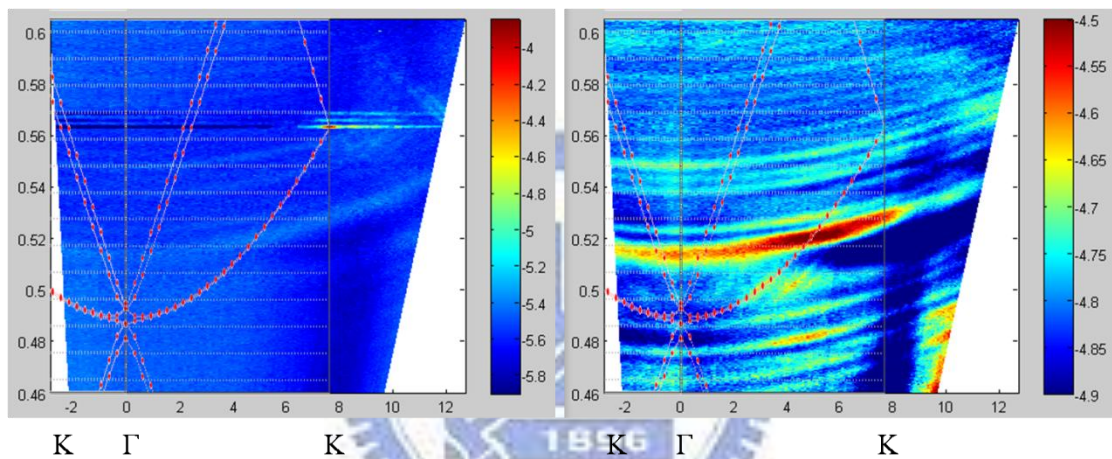observed the PCSEL lasing spot mapped the K2 band-edge mode exactly.

Figure 4-17 The AR μ-PL diagram of K2 mode (Left: pumped by YVO4 pulse laser;

Right: pumped by HeCd laser), the dot-dash line shows band structure.

Divergence angle & Polarization

    As K2 mode must obey the Bragg theory and the energy conservation law, the

lasing angle no more lay in the normal direction but at 29˚. This is coincident with

chapter 2-2. Because of the instrumental limit, the peak intensity angular dependence

in Figure 4-18(a) isn't clear as Γ1 mode (Figure 4-12(a)). If the detector can be

aligned just in the direction normal to the photonic crystal plane without any error, we

believed the peak intensity angular dependence could be increased. The divergence

angle is about 2.5 degree which is much narrower than the VCSELs'. The polarization

shown in Figure 4-18(b) is measured at the maximum peak and the degree of

polarization (DOP) is about 35%. Since the guided mode also extracted by PhCs, the
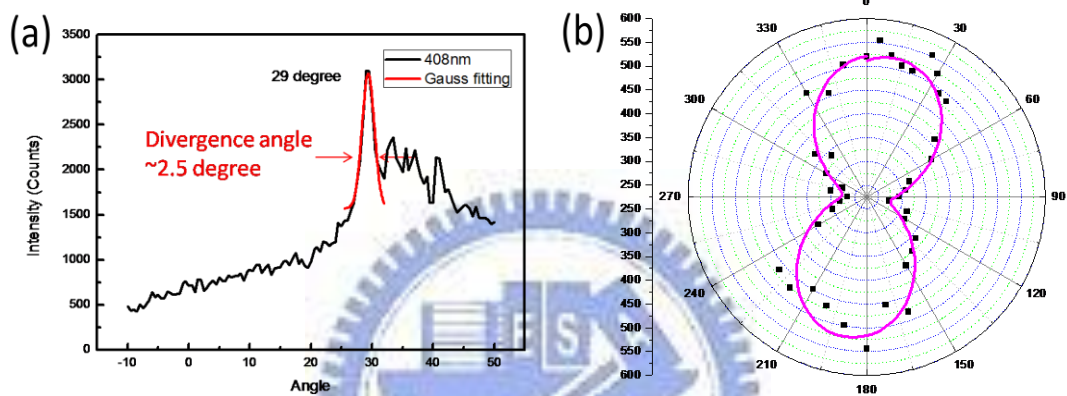
DOP is relatively low as a laser.

Figure 4-18 (a)The divergence angle on the normal plane; (b)The polarization at 29° of K2 mode.

4-4.3 Characteristics of M3 mode GaN-based 2D PCSELs

Lasing action

The r/a ratio (where r is the radius of hole, a is lattice constant) of PhCs is 0.204.

We optical pumped the PCSEL at 77K and the lasing spectrum is shown in Figure

4-20. Since the lattice constant (a) is 230nm, the a/λ ratio is 0.59. Due to the design

for lasing action at M3 device which parameters are described as follows:

$$r/a=0.204, a=230nm, n_b= 2.617, n_a= 1.767, n_{eff}= 2.498$$

put these parameters in R-soft software and plot the band structure (dispersion diagram) for TE-like mode as shown in Figure 4-19. The a/λ ratio observed by experimental result is 0.59 which matched the M3 mode normalized frequency as shown in Figure 4-19. For this reason, we believed this PCSEL lasing at M3 mode.
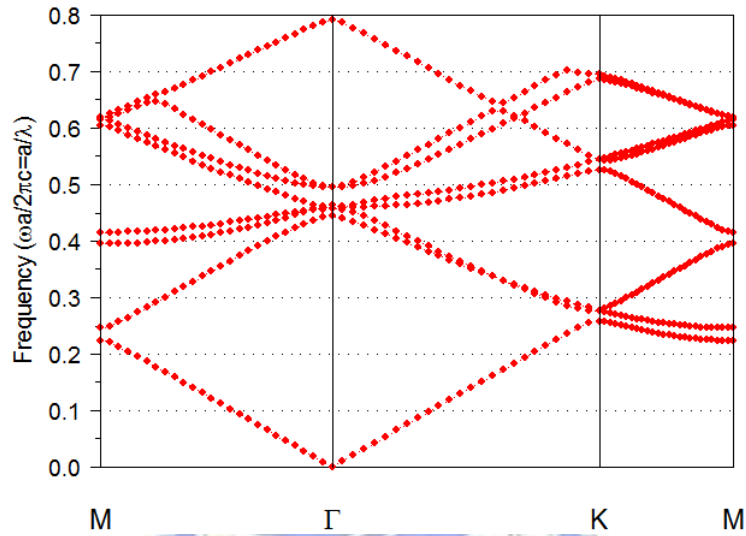

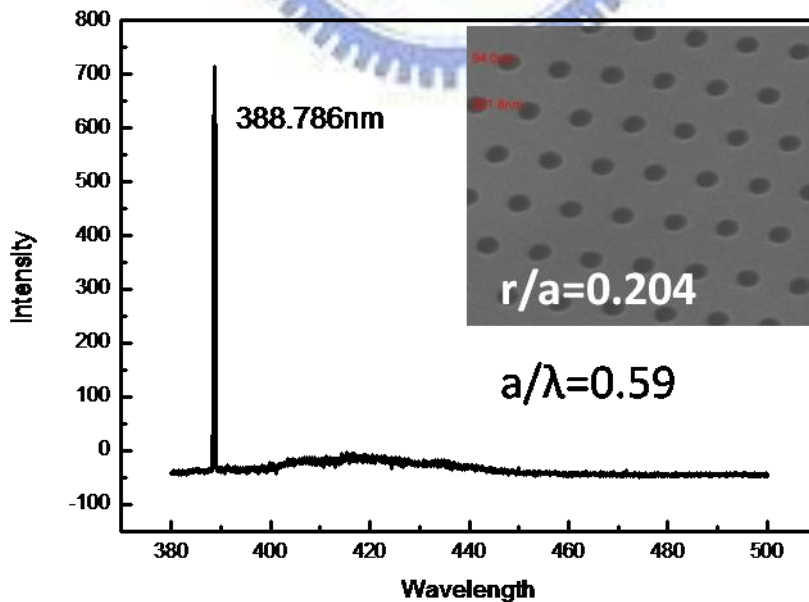**Figure 4-19 The band structure of M3 mode for TE-like mode.**

Figure 4-20 The PL spectrum under lasing action (inset: the SEM image of the PCSELs.

AR μ-PL diagram

Figure 4-21 show the AR μ-PL diagram of M3 mode (Left: pumped by YVO4 pulse laser; right: pumped by HeCd laser) and the dot-dash line shows simulated band structure around M3 mode. By varying the θ defined with respect to the direction normal to the plane and shifting the in-plane direction from Γ to M direction, the photonic band can be mapped with simulated band structure around M3 point. We observed different slopes of diffraction lines in the photonic band. The diffraction lines with different slopes represent different band in the band diagram and we could mapped the band structure with photonic band precisely. Furthermore, we observed the PCSEL lasing spot mapped with the second lowest M3 band-edge mode exactly.
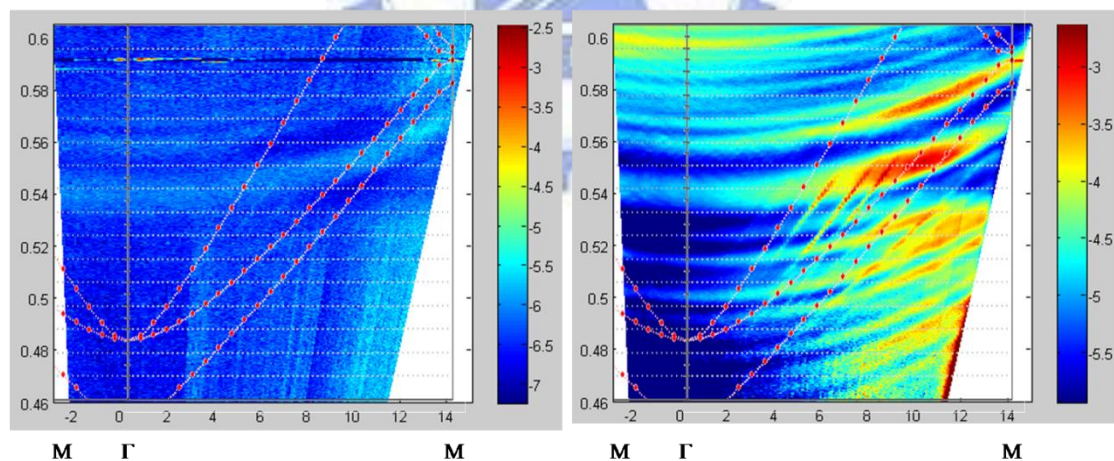

Figure 4-21 The AR μ-PL diagram of M3 mode (Left: pumped by YVO4 pulse laser; Right: pumped by HeCd laser), the dot-dash line shows band structure.

Figure 4-21 is the AR μ-PL diagram of M3 mode. We pumped the PCSEL by both YVO4 laser and HeCd (left and right diagram, respectively) laser in order to

investigate the light intensity distribution in K-space under two conditions: above

lasing and below lasing action arisen, respectively. After mapping the diagram with

band structure, we observed three different slopes of diffraction lines matched with

band structure and the PCSEL lasing at the second lowest mode.

Divergence angle & Polarization

As M3 mode must obey the Bragg theory and the energy conservation law, the

lasing angle no more lay in the normal direction but at 59.5°. This is coincident with

chapter 2-2. The divergence angle is about 2.5 degree which is much narrower than

the VCSELs'. We considered the intensity distribution of emission angle at 55° is

caused by the symmetric far-field pattern of M3 mode. Because of the instrumental

limit we couldn't observe the far-field pattern of M3 mode, we expected we could

prove this statement in the future. The polarization shown in Figure 4-22(b) is

measured at the maximum peak and the degree of polarization (DOP) is about 55%.

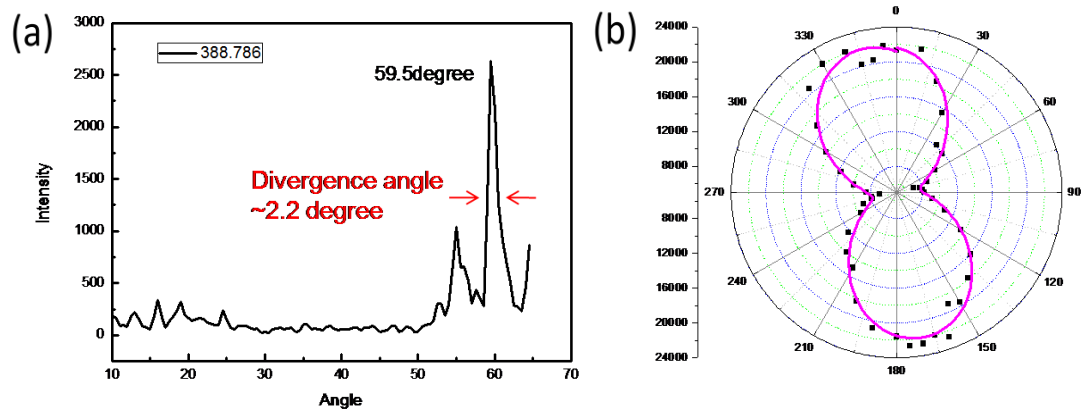Since the guided mode also extracted by PhCs, the DOP is relatively low as a laser.

Figure 4-22 (a)The divergence angle on the normal plane; (b)The polarization at 59.5 degree of M3 mode.

References

[1] Fre´de´ric S. Diana, Aure´lien David, Ines Meinel, Rajat Sharma, Claude

Weisbuch, Shuji Nakamura, and Pierre M. Petroff, *Nano Lett.* **6**, 1116-1120

(2006)

[2] Shing-Chung WANG_, Tien-Chang LU, Chih-Chiang KAO, Jong-Tang CHU,

Gen-Sheng HUANG, Hao-Chung KUO, Shih-Wei CHEN, Tsung-Ting KAO,

Jun-Rong CHEN, and Li-Fan LIN, *Jpn. J. Appl.Phys.*, **46**, 8B, 5397–5407 (2007)

[3] Chih-Chiang Kao, Y. C. Peng, H. H. Yao, J. Y. Tsai, Y. H. Chang, J. T. Chu, H.

W. Huang, T. T. Kao, T. C. Lu, H. C. Kuo, and S. C. Wang, *Appl. Phys. Lett.*, **87**,

081105 (2005)

[4] Tien-Chang Lu, Shih-Wei Chen, Li-Fan Lin, Tsung-Ting Kao, Chih-Chiang Kao,

Peichen Yu, Hao-Chung Kuo, and Shing-Chung Wang, *Appl. Phys. Lett.*, **92**,

011129 (2008)

[5] Masahiro Imada, Alongkarn Chutinan, Susumu Noda, and Masamitsu Mochizuki,

Phys. Rev. B 65, 195306 (2002)

Chapter 5

Conclusion

The GaN-based 2D photonic crystal surface emitting lasers are fabricated and measured in this thesis. The lasing action is achieved under the optical pumping system at 77 Kelvin degree. Normalized frequency of investigated PhCs lasing wavelength can correspond to three band-edge frequencies (Γ1, K2, M3), which indicates the lasing action can only occur at specific band-edges. Angle-resolved μ-PL diagrams confirm the existence of lasing modes at different band-edge (Γ1, K2, M3) by mapping the diffraction patterns with band structures. The three band-edge frequencies (Γ1, K2, M3) has different emission angle in the normal direction (0˚, 29˚, 59.5˚), respectively. The Bragg theory confirms the mechanism of the different emission angles. The far field pattern of Γ1 mode is symmetric due to the PhCs' symmetric pattern design. Besides, the degree of polarization and divergence angle of the (Γ1, K2, M3) mode laser emission is about (33%, 35%, 55%) and (1.2˚, 2.5˚, 2.2˚), respectively.

We will further improve the fabrication techniques of GaN PCSEL to achieve the laser operation by electrically pumped using high transparent contact and current blocking. Moreover, the research of GaN-based defect mode PhCs laser becomes a

hot topic according to its specific advantages compared with band-edge mode PhCs

laser. Therefore, we will also investigate the characteristics of GaN-based defect mode

PhCs laser.